

MORPHOLOGY, STRUCTURE, AND TECTONIC EVOLUTION OF THE MONA
CANYON, PUERTO RICO

Steven A. Mondziel

A Thesis Submitted to the
University of North Carolina Wilmington in Partial Fulfillment
Of the Requirements for the Degree of
Master of Science

Department of Geography and Geology

University of North Carolina Wilmington

2007

Approved by

Advisory Committee

Chair

Accepted by

Dean, Graduate School

This document has been prepared according to the guidelines for submission to the
Journal of Marine Geology

TABLE OF CONTENTS

ABSTRACT	v
ACKNOWLEDGEMENTS	vii
LIST OF TABLES	ix
LIST OF FIGURES	x
INTRODUCTION	1
Overview and Significance of the Research	1
Pinning and Extension Model	4
Rotating Block Model	5
Incised Canyon Model	7
BACKGROUND	10
Geologic and Tectonic Setting	10
Previous Studies	11
MARINE GEOPHYSICAL DATA AND METHODOLOGY	16
Multibeam Bathymetry Data	16
Single-Channel Seismic Reflection Data	19
Multi-Channel Seismic Reflection Data	20
Interpretation of Single- and Multi-Channel Seismic Reflection Data	21
Earthquake Data	28
RESULTS AND INTERPRETATION OF MARINE GEOPHYSICAL DATA	29
Morphology and Structure	29
Southern Mona Canyon	30
Central Mona Canyon	35

Northern Mona Canyon and Mona Block.....	40
STRUCTURAL RESTORATION OF CENTRAL MONA CANYON.....	53
DISCUSSION.....	60
Comparison of Evidence with Proposed Tectonic Models.....	60
Pinning and Extension Model.....	60
Rotating Block Model.....	66
Incised Canyon Model	67
Summary of Tectonic Models.....	69
Tectonic Evolution of Central Mona Canyon.....	69
Tectonic Phase I: Initial Rifting in Central Mona Canyon: Middle Oligocene to Late Miocene	71
Tectonic Phase II: Later Rifting in Central Mona Canyon: Late Miocene to Recent	76
Tsunami Implications.....	78
CONCLUSIONS.....	85
REFERENCES	87

ABSTRACT

The Mona Canyon is a z-shaped, 20-30 km-wide, 140 km-long, and 2-3.5 km-deep atypical submarine canyon that incises the Greater Antilles island arc off the northwest coast of Puerto Rico. This is the first study to systematically integrate multiple sets of marine geophysical data, including multibeam bathymetry, sidescan sonar imagery, single- and multi-channel seismic reflection profiles, and earthquakes to evaluate the morphology, structure, and the tectonic evolution of the Mona Canyon. The data suggest that the Mona Canyon is a half-graben structure that is controlled by the listric Mona Canyon master fault on the east side of the canyon, and antithetic faults on the west side of the canyon.

The interpreted marine geophysical data leads to a proposed extensional model for the formation of the Mona Canyon. A structural restoration of the central Mona Canyon performed in this study indicates that extension in the Mona Canyon appears to have initiated in the Middle Oligocene, approximately 30 Ma. This is in contrast to the previous estimate of 1.2 Ma that was predicted using differential GPS vectors between Hispaniola and Puerto Rico. The extension is proposed to have occurred over two phases. Phase I occurred from the Middle Oligocene to Late Miocene, and was a slow, initial stage of at least 1.66 km. Phase II occurred from the Late Miocene to the Recent, and was a more rapid, late stage extension of at least 4.39 km, for a total minimum extension through the Recent of 6.05 km.

On October 11, 1918, a M7.2 earthquake near the southern end of the Mona Canyon generated a 4-6 m-high tsunami that inundated the northwest coast of Puerto Rico, and claimed over 100 lives. This study presents evidence for a 7 km-wide, 200 m-

high amphitheater-shaped headscarp in the southern Mona Canyon that is located in the same region as two submarine cable breaks that occurred after the 1918 tsunami.

Numerical modeling performed using the southern Mona Canyon mass wasting feature as a source mechanism for the deadly 1918 tsunami generates a wave that matches well with the observed 4-6 m-high run-up, phase, and timing.

ACKNOWLEDGEMENTS

I would like to first thank my committee members, Drs. Nancy Grindlay, Lew Abrams, and Dave Blake for their guidance and support throughout my stay at University of North Carolina Wilmington (UNCW). I would also like to thank Dr. Paul Mann at the University of Texas at Austin Institute for Geophysics (UTIG) for being an outside reader of this Master's thesis. I would like to thank Roger Shew for his willingness to help me interpret my seismic data, as well as helping me become an experienced teacher, and subsequently, a much better geologist and public speaker. I would also like to thank Catherine Morris and Anne Sutter for their logistical support, as well as for being the backbone of the UNCW Geography and Geology Department.

I would like to thank Drs. John Diebold and Neil Driscoll at the Lamont-Doherty Earth Observatory (LDEO) for allowing access to the EW9501 multi-channel seismic (MCS) data. I would like to thank Joyce Alsop at LDEO and Lisa Gahagan at UTIG for facilitating the transfer of the EW9501 data. I would like to thank Steffen Sastrup and Dr. Kirk McIntosh for helping me to process the three EW9501 MCS lines at UTIG in an incredibly short time period. I would like to thank Dr. Alejandro Escalona for providing his expertise in seismic interpretation and structural restorations. I would like to thank Drs. Katherine Ellins and Sabine Wulf for providing me with residence during my stay in Austin, Texas. I would also like to thank Dr. Matthew Hornbach for his help in the tsunami aspects of this thesis.

Finally, I would like to thank my family and friends for providing me with the two most important kinds of support, emotional and monetary, throughout my education. Without them, none of this would have been possible.

This research has been partially supported by the U.S. National Science Foundation (OCE-9796189 (NRG) and OCE-9504118 (PM)), University of Puerto Rico SeaGrant Program (R-122-1-04 (NRG)), the UNCW Center for Marine Science, and the UNCW Geography and Geology Department.

LIST OF TABLES

Table 1: Combined multibeam bathymetry data collected over the Mona Canyon and used in this study.....	17
---	----

LIST OF FIGURES

Fig. 1. Bathymetric and tectonic index map of a portion of the northeast Caribbean	2
Fig. 2. Pinning and extension model.....	6
Fig. 3. Rotating block model.....	8
Fig. 4. Incised canyon model	9
Fig. 5. Detailed shaded-relief bathymetric and tectonic map over the Mona Canyon study area showing major structures and locations of seismic tracklines, dredges/cores, and NR-1 and DSRV/Alvin dives.....	12
Fig. 6. Stratigraphic columns and correlation of well logs	22
Fig. 7. Reflector characteristics used in SCS and MCS interpretation	24
Fig. 8. Across-axis bathymetric profiles 1-9 and along-axis composite bathymetric profile A-B-C-D.....	31
Fig. 9. EW9605 SCS Line 32.....	33
Fig. 10. Generalized geologic map of Mona Canyon study area.....	36
Fig. 11. EW9501 MCS Line 1289	39
Fig. 12. Detailed view of seismic stratigraphy over central Mona Canyon.....	41
Fig. 13. EW9605 SCS Line 25.....	42
Fig. 14. EW9501 MCS Line 1290	45
Fig. 15. EW9501 MCS Line 1291.	47
Fig. 16. EW9605 SCS Line 27.....	48
Fig. 17. EW9605 SCS Line 29.....	50
Fig. 18. Structural restoration of interpretation of EW9501 MCS Line 1289 over central Mona Canyon.....	55

Fig. 19. Earthquake-fault map over Mona Canyon..... 62

Fig. 20. Vertical earthquake profile across the Puerto Rico trench and the Greater
Antilles island arc 64

Fig. 21. Plate tectonic reconstructions of the northeast Caribbean Puerto Rico trench –
SE Bahamas collision zone for four intervals..... 72

Fig. 22. Southern Mona Canyon mass wasting feature 82

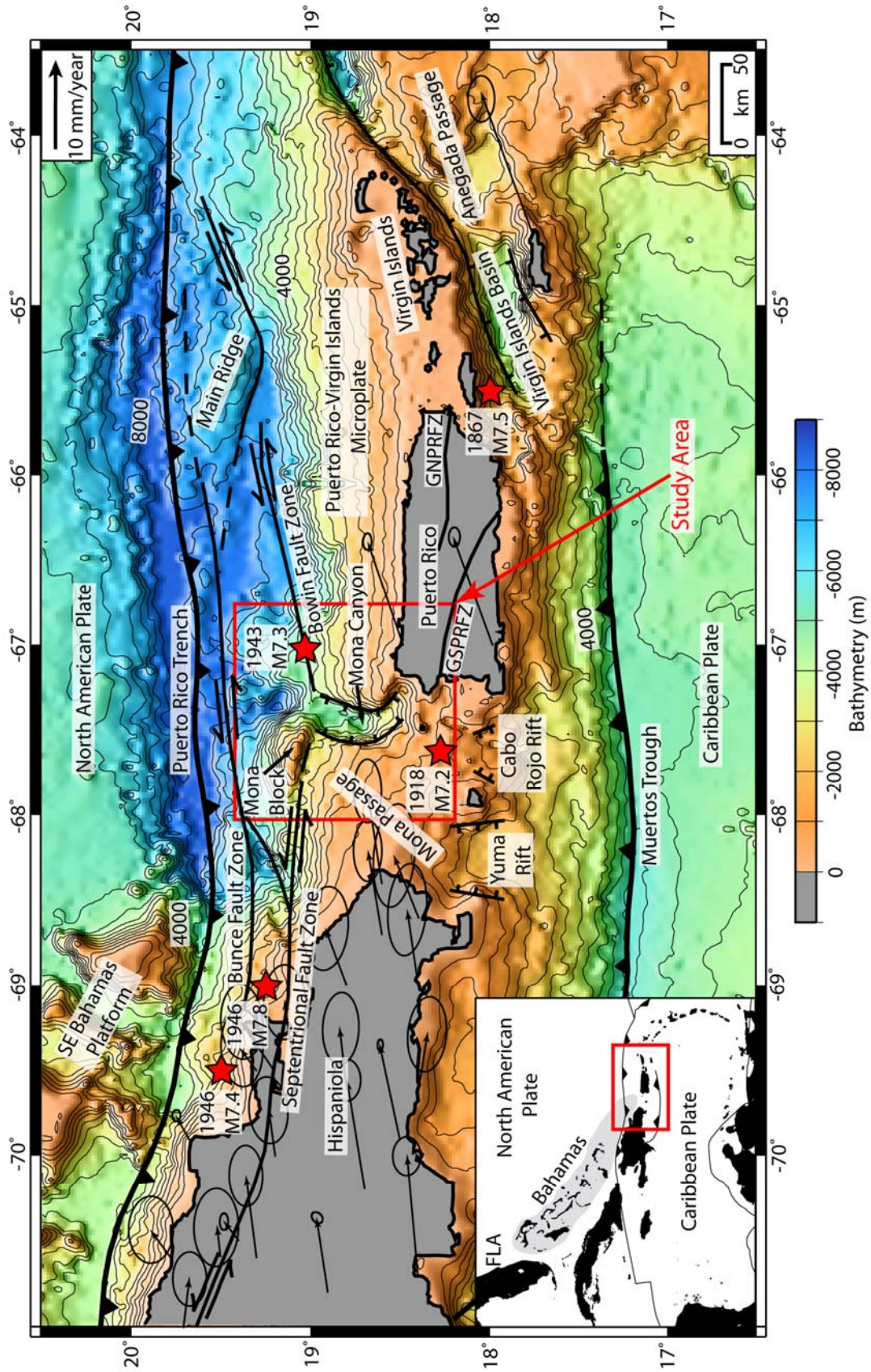
INTRODUCTION

Overview and Significance of the Research

The Mona Canyon is a north-south-trending, 20-30 km-wide, 140 km-long, and 2-3.5 km-deep submarine canyon that incises the Late Cretaceous Greater Antilles island arc in the Mona Passage marine strait offshore northwest Puerto Rico (Fig. 1). The Mona Canyon appears to be geologically different from other submarine canyons found along the U.S. continental margin, such as the Monterey and Hudson canyons, as well as the Arecibo, Quebradillas, and Tiberones canyons on the northern margin of Puerto Rico (Gardner et al., 1980; Shepard, 1981). Rivers during sea level low stands and/or turbidity currents are considered to carve most submarine canyons, making them purely erosional features. However, the lack of any rivers that empty into the canyon, as well as dramatic changes in gradient, trend, underlying lithology and structure, and frequent shallow earthquakes suggest the Mona Canyon has experienced a complicated geologic history.

On October 11, 1918, an approximately M7.2 earthquake 40 km off the northwestern coast of Puerto Rico, initially located at the southern end of the Mona Canyon (Fig. 1), generated a 4-6 m-high tsunami that inundated the northwest coast of Puerto Rico (Reid and Taber, 1919; Mercado and McCann, 1998). The combination of Intensity IX ground-shaking and the subsequent tsunami resulted in the deaths of at least 116 people, and caused more than \$45 million in damage (adjusted to current \$US; Reid and Taber, 1919; Mercado and McCann; 1998). The population of Puerto Rico has greatly increased from 1918 to 2007, now approaching four million inhabitants in a 7000 km² area, making it one of the most densely populated regions in the Western Hemisphere (Mann, 2005). Seventy-three percent of inhabitants live in four major cities

Fig. 1. Bathymetric and tectonic index map of a portion of the northeast Caribbean. Map depicts topography, structure, GPS-based plate motions relative to North America, and major historical earthquakes. Inset map for reference; shaded gray area represents extent of Bahamas carbonate platform. Red box outlines study area. Illumination is from the north. Faults are from Grindlay et al. 2005. GSPRFZ – Great Southern Puerto Rico Fault Zone, GNPRFZ – Great Northern Puerto Rico Fault Zone. Red stars show the locations of significant historical earthquakes from Pacheo and Sykes (1992), Dolan and Wald (1998), and Doser et al. (2005). GPS velocities relative to North America that have two-dimensional 95% confidence ellipses are from Calais et al. (2002).



on the northern, San Juan and Arecibo, and western, Aguadilla and Mayaguez, coastal areas of the island where the devastating tsunami struck 89 years ago.

Because of the lack of an integrated marine geophysical data set that includes both seafloor surface and subsurface data, the origin of the tectonically active Mona Canyon remains poorly understood. Moreover, key information required for accurate seismic and tsunami hazard potential and susceptibility, such as the nature and distribution of active and reactivated fault structures, and their relationship to possible mass wasting scarps and shoreline geomorphology, is unknown.

This study processes, interprets, and correlates an extensive set of marine geophysical data collected on various NSF-, UTIG-, and NOAA-supported research cruises from the decade 1995-2005. These data sets include high-resolution multibeam bathymetry, sidescan sonar imagery, and single- and multi-channel seismic reflection profiles over the Mona Canyon. Combined with earthquake seismicity data such as first motion studies and historical and recent shallow earthquake locations, these data make it possible to investigate the locations of active faults, characterize the style of past and recent deformation, and identify areas of slope instability in the Mona Canyon.

This study uses the newly integrated data to test three tectonic models for the origin of the Mona Canyon:

Pinning and Extension Model

It is hypothesized that the southeast end of the 22-27 km-thick Bahamas carbonate platform and oceanic crust sequence on the North American plate began obliquely subducting into the Puerto Rico trench north of Cuba in the Eocene. Due to the highly

oblique transpression, the southeast end of the Bahamas is interpreted to have subducted beneath the northern Puerto Rico margin from northeast to southwest beginning in the Late Miocene to Late Pliocene, approximately 11-3 Ma (McCann and Sykes, 1984; Dolan et al., 1998; Dolan and Wald, 1998; Mann et al., 2002; McCann, 2002; Grindlay et al., 2005; Mann, 2005). The current subduction zone is offshore northwest Puerto Rico (Fig. 1). This subduction is inferred to have led to the formation of the Mona Block, which is an anomalous shallowing of the forearc that appears to extend from the southeast-trending lineament of the Bahamas platform (Fig. 1). A high concentration of recent earthquakes accompanies this localized asymmetric bathymetric high (Perfit et al., 1980; Heezen et al., 1985; McCann and Sykes, 1984; McCann 2002; Grindlay et al., 2005). It is also hypothesized that the Bahamas Platform is too thick and buoyant to continue to subduct, thereby pinning Hispaniola and allowing Puerto Rico and the Virgin Islands to drift away to the east as a microplate through transtension. The Mona Canyon would therefore represent an east-west extending structural graben between the pinned Hispaniola and unpinned Puerto Rico and Virgin Islands (Fig. 2); (Mann et al., 2002; Grindlay et al., 2005; Hippolyte et al., 2005; Jansma and Mattioli, 2005).

Rotating Block Model

Geist et al. (1988) and Dobson et al. (1996) suggest that the formation of submarine summit basins and transverse canyons in the Aleutian island arc follow a rotating block model. There, oblique dextral convergence of the Pacific plate beneath the North American plate results in partitioning of the forearc into rhombic crustal blocks. Subsiding, dextral, tear fault-controlled summit basins that open into deeper transverse

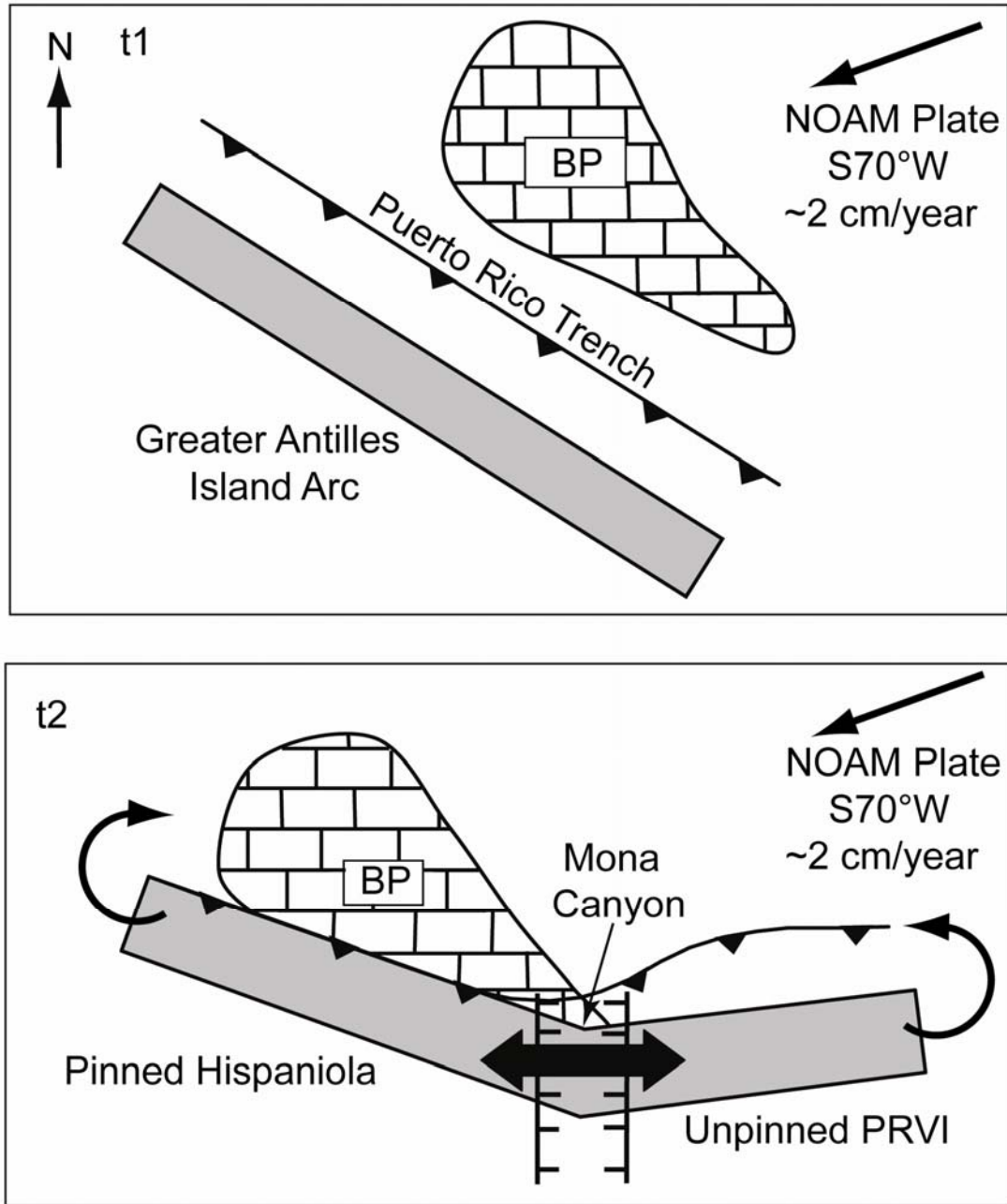


Fig. 2. Pinning and extension model. Modified after Mann et al. (2002). Oblique collision of the 22-27 km-thick Bahaman Platform (BP) with Greater Antilles Island Arc in the Eocene (t1) results in the partitioning of the island arc into microplates by transension and normal faulting in the Mona Passage (MP), and the formation of the Mona Canyon between the pinned and unpinned regions through the Recent (t2). NOAM Plate – North American plate.

canyons between the rotated portions of the island arc massif bound the rhombic blocks. The dip-slip and strike-slip faults result from arc-normal extension and massive amphitheater-shaped headscarps resulting from mass wasting processes border the canyons (Geist et al., 1988; Dobson et al., 1996). The rotating block model is hypothesized to be responsible for the formation of the Mona Canyon, and its application to the study area is shown in Fig. 3.

Incised Canyon Model

Laursen and Normark (2002) describe a neotectonic setting similar to the Mona Canyon that is located in the central Chile forearc. Using an incised canyon model, they propose that the oblique subduction of the Topocalma Knoll seamount into the Peru-Chile trench caused the formation of the San Antonio submarine canyon. Continued underthrusting of this seamount results in bulging, arching, and oversteepening beyond the angle of repose for the forearc strata. Continued underthrusting allows the canyon to evolve through headward erosion of a reentrant. Evidence for this erosion sequence includes amphitheater-shaped headscarps and ponded turbidite deposits throughout the canyon (Laursen and Normark, 2002). The incised canyon model is hypothesized to be responsible for the formation of the Mona Canyon, and its application to the study area is shown in Fig. 4.

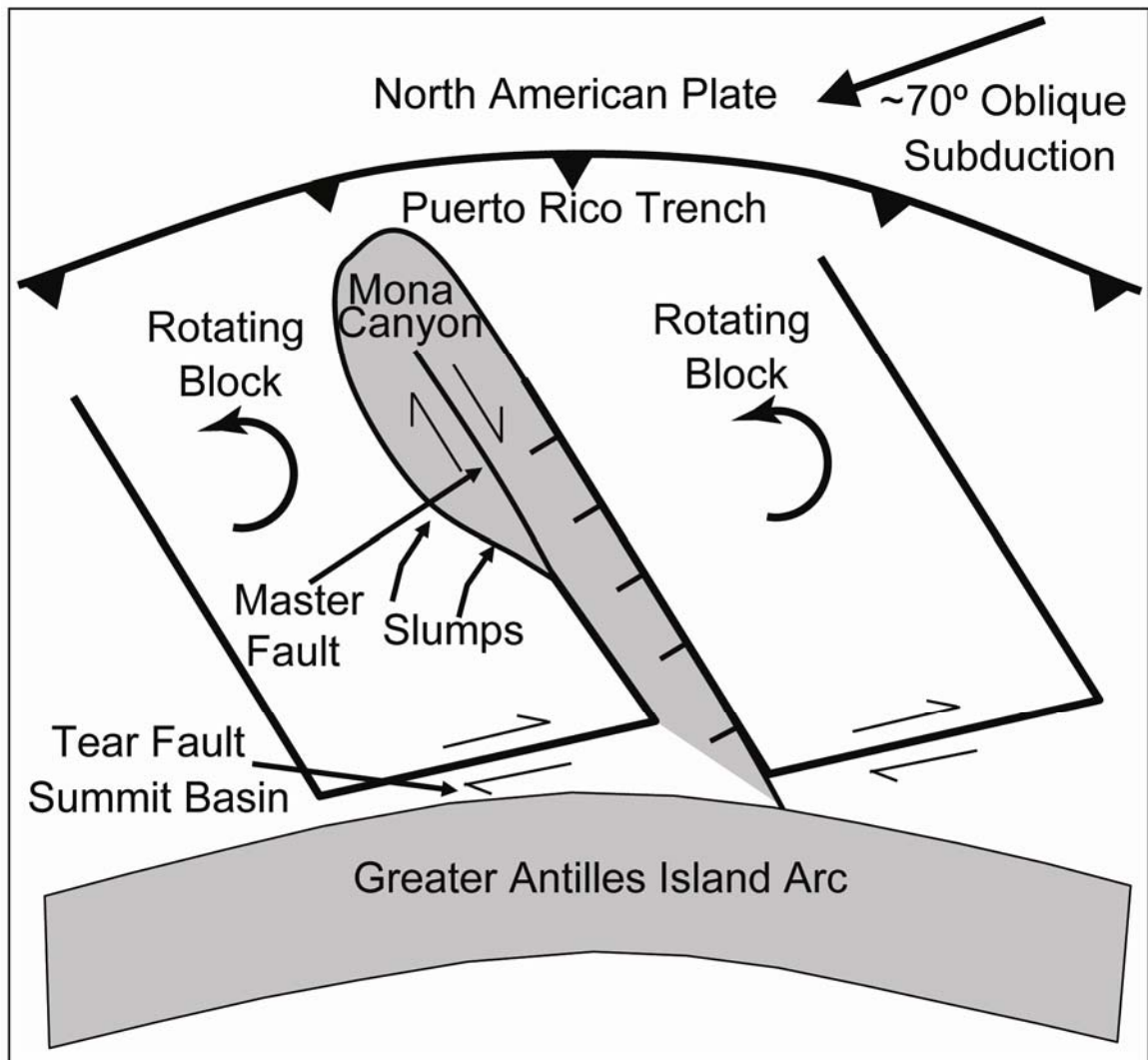


Fig. 3. Rotating block model. Modified after Geist et al. (1988) and Dobson et al. (1996). Highly oblique subduction results in the partitioning of the forearc into rhombic crustal blocks. Triangular-shaped tear fault summit basins and dextral transverse canyons bound the rhombic blocks.

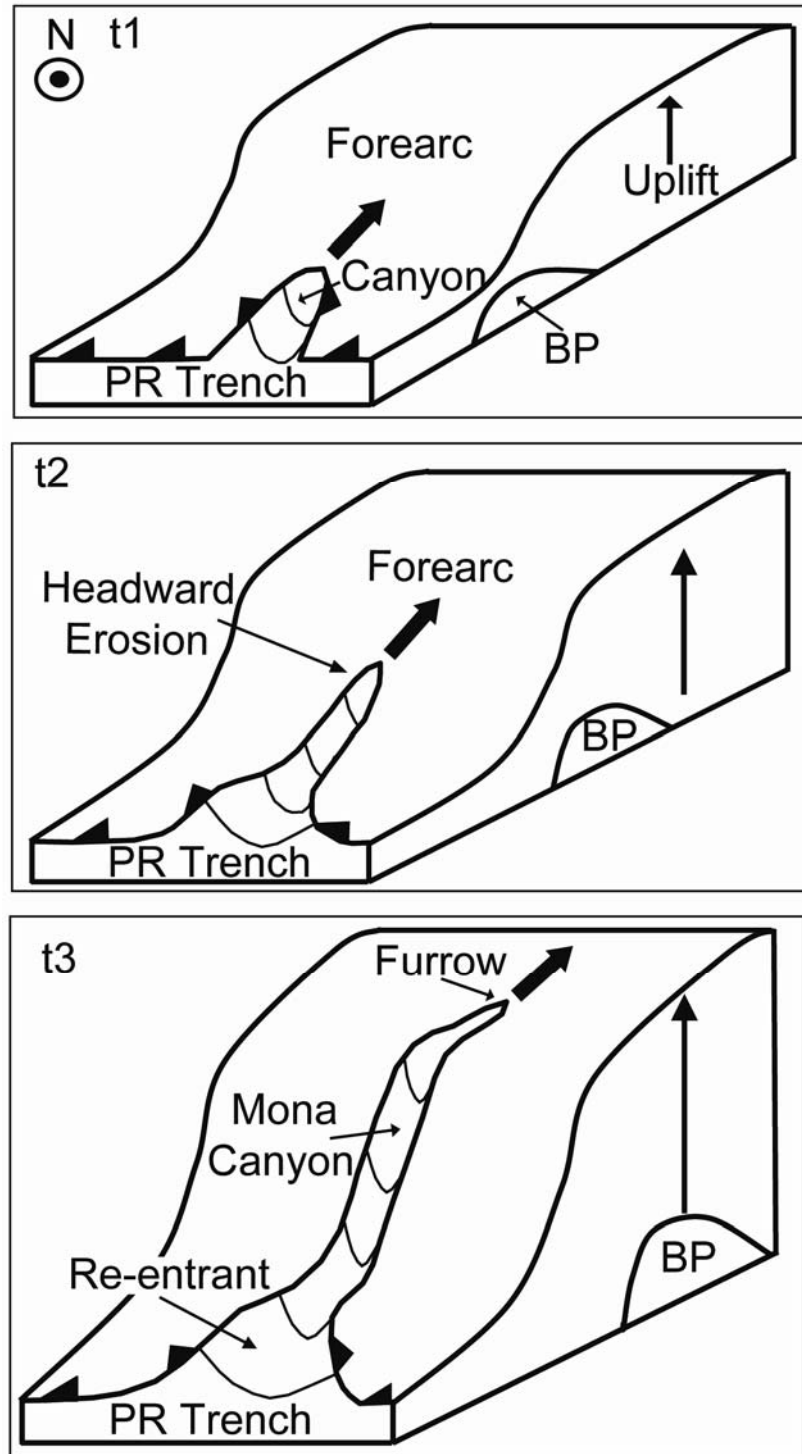


Fig. 4. Incised canyon model. Modified after Laursen and Normark, 2002. Underthrusting of 22-27 km-thick Bahaman Platform (BP) into the Puerto Rico (PR) trench causes bulging and uplift of forearc region, eventually resulting in oversteepening beyond angle of repose for the forearc strata. Continued subduction leads to the headward erosion of a reentrant, resulting in the formation of a submarine canyon.

BACKGROUND

Geologic and Tectonic Setting

The island of Puerto Rico is situated in the volcanically extinct Greater Antilles island arc in the narrow and complex transitional tectonic plate boundary zone between the North American and Caribbean plates (Fig. 1). The North American plate is currently subducting into the Puerto Rico trench at a rate of approximately 2 cm/yr in a direction of $S70^{\circ}W$ (Mann et al., 2002). The relative plate motion is therefore sinistral with minor oblique thrusting, creating a sinistral transpressional plate boundary (Jansma et al., 2000; Mann et al., 2002). This deformation is accommodated by the northeast-trending, sinistral Bowin, Bunce, and Septentrional fault zones (Fig. 1); (Grindlay et al., 2005).

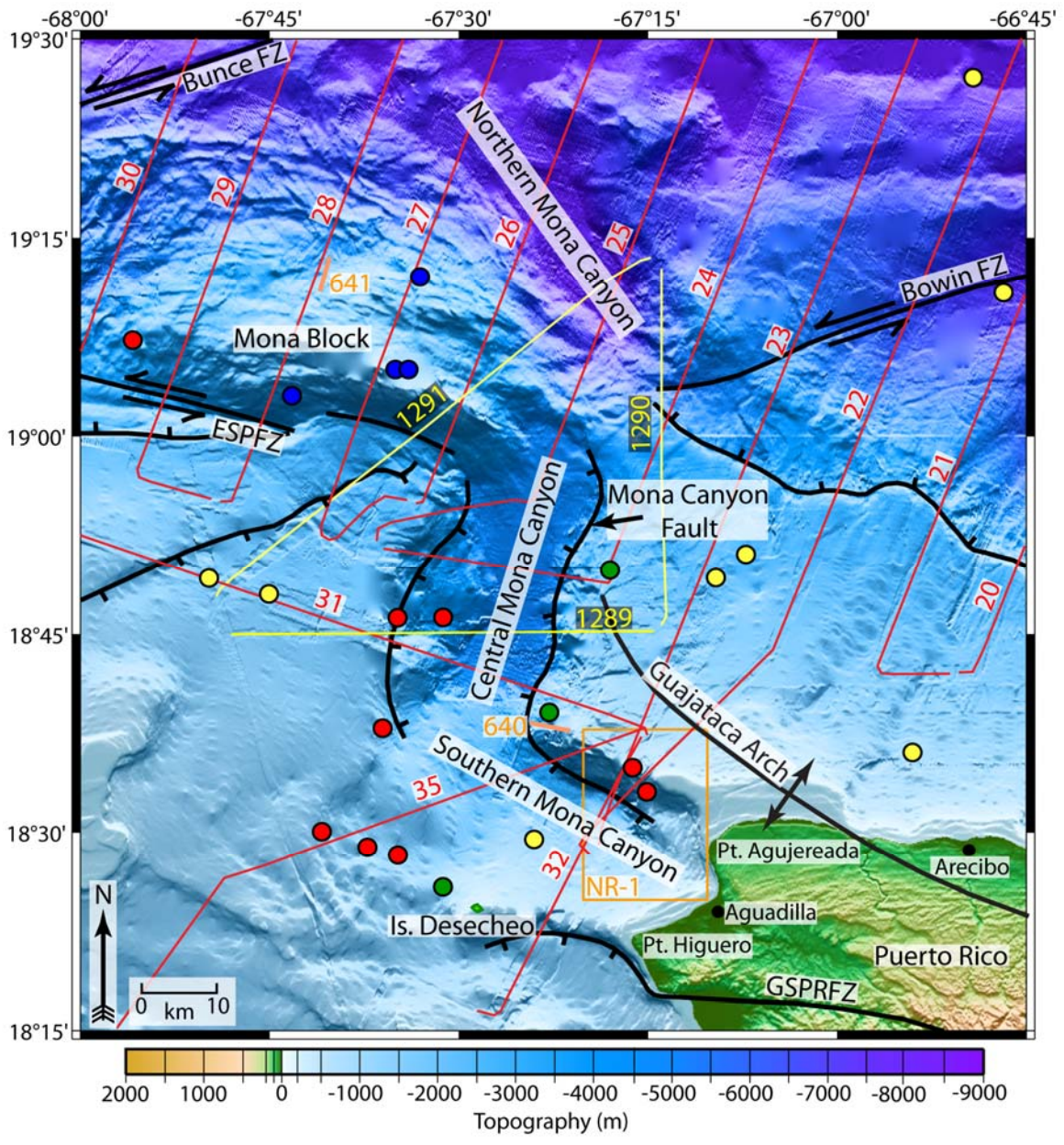
Puerto Rico and the Virgin Islands form the Puerto Rico-Virgin Islands (PRVI) microplate, which is the easternmost microplate within this transitional plate boundary zone (Fig. 1). Structurally active geomorphic features that accommodate the plate deformation in this zone bound all four sides of the PRVI microplate. The northern boundary of the PRVI microplate is the Puerto Rico trench, which defines the southern edge of the subducting North American plate, and has the location of the deepest point in the Atlantic Ocean at approximately 8400 m (Masson and Scanlon, 1991). The southern boundary is the Muertos Trough, and is a zone of subduction that marks the northern edge of the Caribbean plate (Fig. 1); (Ladd et al., 1977). The eastern and western edges of the PRVI microplate are the Anegada Passage and the Mona Passage marine straits, respectively (Fig. 1); (Masson and Scanlon, 1991; Jansma et al., 2000, LaForge and McCann, 2005). The Mona Canyon is situated on the southern (i.e. landward) slope of the Puerto Rico trench at the north end of the Mona Passage marine strait.

Previous Studies

Fox and Heezen (1975) and Perfit et al. (1980) cored and dredged surficial sediments around the north-trending Mona Canyon in an effort to evaluate the geology of the Puerto Rico trench (Fig. 5). Gardner et al. (1980) used the Nuclear Research Submarine NR-1 to examine the rocks and map active faults in the southern part of the Mona Canyon off the northwest coast of Puerto Rico (Fig. 5). In 1976, the DSRV/Alvin made dives #640 and #641, in the southern part of Mona Canyon and the northwest flank of Mona Block forearc uplift, respectively (Fig. 5); (Heezen et al., 1985).

Using the NR-1 submarine, Gardner et al. (1980) observed a 20-70 m-thick sequence of unconsolidated terrigenous and calcareous sediments shed off the northwest coast of Puerto Rico covers the floor of the southern Mona Canyon, although there are no rivers that empty directly into the canyon. Gardner et al. (1980) noted ponded turbidites in the axis are transitional into larger rock rubble and 1-2 m angular talus blocks towards the steep, 45° east wall of the canyon. These blocks have sharp edges and lack any sediment covering or fault scarp-fill, suggestive of recent structural activity (Gardner et al., 1980; Heezen et al., 1985). Gardner et al. (1980) and Heezen et al. (1985) also note that the east wall of the canyon has a cliff-and-bench topography composed of Late Cretaceous to Middle Eocene zeolite to greenschist facies metavolcanic and metaplutonic rocks. Shallow water limestone of the Middle Oligocene to Late Miocene/Early Pliocene PRVI carbonate platform overlay the basement rocks. Subaerial karst processes and extensive faulting overprint both sequences (Heezen et al., 1985). In contrast to the steep east wall of the Mona Canyon, its south and west walls have only a 10° slope on average with a cliff-and-bench topography, and are composed of presumably identical

Fig. 5. Detailed shaded-relief bathymetric and tectonic map over the Mona Canyon study area showing major structures and locations of seismic tracklines, dredges/cores, and NR-1 and DSRV/Alvin dives. The study area is outlined by the red box in Fig. 1. Illumination is from the south. Map generated using hydrosweep bathymetric data shown in Table 1, which is supplemented with recent coastal relief measurements from the NOAA National Geophysical Database Center (NGDC). EW9605 single-channel seismic reflection tracklines are shown in red, EW9501 multi-channel seismic reflection tracklines are shown in yellow. Orange lines are locations of DSRV/Alvin dives #640 and #641 (Heezen et al., 1985). Orange box is region of NR-1 submarine dives (Gardner et al., 1980). Filled circles are locations of dredges after Fox and Heezen, 1975; Perfit et al., 1980; Heezen et al., 1985: green = greenschist facies island arc volcanic and volcanoclastic basement rocks, red = limestone, blue = blueschist facies calcsilicate schist and marble, yellow = unconsolidated sediments. Black lines are major structural lineaments. Faults shown are active features with seafloor relief. ESPFZ – East Septentrional Fault Zone, GSPRFZ – Great Southern Puerto Rico Fault Zone (Grindlay et al., 2005).



carbonate strata that overlay island arc volcanic and volcanoclastic basement rocks (Gardner et al., 1980; Heezen et al., 1985; Larue and Ryan, 1989).

DSRV/Alvin Dive #641 was located on the northwest flank of the Mona Block, and documented a greater than 300 m-wide section of a Pleistocene lagoonal patch reef at 3652 m depth that lacked any manganese coating. They therefore concluded it had been transported to this depth by recent mass wasting processes, such as slumping (Heezen et al., 1985). Researchers on the dive noted the north wall of the Mona Block also displays a cliff-and-bench topography composed dominantly of calcsilicate schist and marble, similar to a Late Cretaceous to Middle Eocene blueschist terrane that crops out on the Samana Peninsula in northeastern Hispaniola first described by Joyce (1991). Dredging in the area of the Mona Block also recovered identical blueschist facies calcsilicate schist and marble (Fig. 5); (Perfit et al., 1980; Heezen et al., 1985).

Previous studies indicate that several sets of north- and northwest-trending normal-slip and oblique-slip faults control the Mona Canyon (Fig. 5); (Gardner et al., 1980; Perfit et al., 1980; Heezen et al., 1985; Larue and Ryan, 1989; Mercado and McCann, 1998; Grindlay et al., 2005; LaForge and McCann, 2005). North-trending normal faults that have hundreds to thousands of meters of displacement and overprint volcanic and volcanoclastic basement rocks control the abrupt and steep east wall of the Mona Canyon (Gardner et al., 1980; Perfit et al., 1980; Heezen et al., 1985; Larue and Ryan, 1989). These structures include the north-trending Mona Canyon fault, which has normal-slip or oblique-slip displacements (Fig. 5); (Mercado and McCann, 1998). These structures are presumably responsible for creating the cliff-and-bench, block-faulted topography on the east wall of the Mona Canyon.

The Mona Canyon has been previously interpreted as a half-graben by Larue and Ryan (1989) and as a simple full graben by Mann et al. (2002). Paleostress studies and slip-vector analyses indicate the Mona Canyon is experiencing E-W extension (Jansma et al., 2000; Mann et al., 2002; Hippolyte, et al., 2005). Geodetic measurements have constrained the rate of E-W extension in the northern Mona Passage to approximately 0.5 cm/yr. If this rate is held constant for its entire evolution, this suggests that the Mona Canyon is approximately 1.2 million years old (Jansma et al., 2000; Mann et al., 2002).

MARINE GEOPHYSICAL DATA AND METHODOLOGY

Multibeam Bathymetry Data

Multibeam bathymetry data were compiled from numerous sources. Recent coastal relief measurements from the northeast Caribbean supplied by NOAA's online National Geophysical Database Center (NGDC) supplement these data sets (Table 1). All multibeam bathymetry data were ping edited, processed, and merged using MBsystems software to generate a digital terrain model (DTM) of all topographic data sets at a 150-m grid interval. The program Generic Mapping Tools (GMT) was then used to generate plots of the DTMs for detailed analysis. IVS3D DMagic software was used to generate shaded relief maps of the DTMs, and to drape the sidescan sonar imagery over the bathymetric data.

Sidescan Sonar Data

In May and June of 1996, 14 lines of sidescan sonar data over the Mona Canyon study area were collected using the Hawaii Mapping Research (HMR) group's HMR-1 sidescan sonar system as part of research cruise EW9605. This shallow-towed towfish system emits simultaneous frequencies of 11 and 12 kHz from transducers on the sides of the fish to image seafloor reflectivity (i.e. backscatter).

The data were processed by the HMR-1 group, which included noise filtering, slant range and beam angle corrections, and destriping. The processed data were gridded at a 17-m grid interval, and were placed in a georeferenced mosaic using the 1984 World Geodetic Survey (WGS) UTM datum so digital images could be generated. The images were digitally scanned, and the contrast and brightness were enhanced over the study area

Table 1. Combined multibeam bathymetry data collected over the Mona Canyon and used in this study. Recent coastal relief measurements from the NOAA NGDC supplement the multibeam bathymetry data.

TABLE 1: MULTIBEAM BATHYMETRY DATA						
CRUISE	DATE	VESSEL	BATHYMETRY SYSTEM	NUMBER OF LINES	CHIEF SCIENTIST(S)	ARCHIVE LOCATION
EW9501	February 1995	R/V Maurice Ewing	Atlas Hydrosweep DS	3	J. Diebold, N. Driscoll	LDEO
EW9605	May and June 1996	R/V Maurice Ewing	Atlas Hydrosweep DS and HMR-1	8 (Hydrosweep), 5 (HMR-1)	N.R. Grindlay, P. Mann, J. Dolan	UNCW CMS
EW0105	May 2001	R/V Maurice Ewing	Atlas Hydrosweep DS	2	T. Joyce	NOAA NGDC
RB0208	September 2002	R/V Ron Brown	Seabeam 2112	10	Uri ten Brink	NOAA NGDC
RB0303	February 2003	R/V Ron Brown	Seabeam 2112	14	Uri ten Brink	NOAA NGDC
EW0404	April-June 2004	R/V Maurice Ewing	Atlas Hydrosweep DS	1	P. Mann, D.S. Sawyer	UTIG

using Adobe Photoshop. The images were then imported into IVS3D DMagic and draped onto the DTM.

Single-Channel Seismic Reflection Data

Fourteen single-channel seismic (SCS) reflection profiles having a total length of 1966 km were collected over the Mona Canyon study area on cruise EW9605 (Fig. 5). The survey employed a 6 airgun array, yielding a total source volume of 1385 cubic inches at 2000 psi. The shot repetition rate ranged from 16-18 seconds, creating an average shot spacing between 40 and 55 m while maintaining an average ship speed of 5-6.5 knots. The towed streamer consisted of 4 channels having a source to near channel offset of 177 m. Because the distance between the near and far channel was only 106.25 m, and the average depth of the seafloor is 5 km, the difference in signal arrival time between channel 1 and 4 is on the order of 2 milliseconds (ms), which is equal to the sampling rate. Therefore, the data were stacked without moveout corrections prior to being put to tape.

The 14 EW9605 SCS lines were processed in April, 2007 at the UNCW Center for Marine Science (CMS) using Parallel Geoscience's Seismic Processing Workshop (SPW) software. Each line utilized the following processing sequence: 1) convert data from SEG-Y format into SPW format, 2) edit data of missing and noisy shots, 3) apply single 100 ms gap deconvolution operator, 4) stolt migration using water velocity (1500 m/s), 5) apply time variant bandpass filter (10-26-100-120 Hz), 6) mute water column, and 7) apply 5 dB pre-rasterization gain. The final processed data were exported as true amplitude bitmaps for interpretation in Adobe Illustrator.

Multi-Channel Seismic Reflection Data

In February 1995, researchers on cruise EW9501 aboard the R/V Maurice Ewing collected three high-resolution, deep penetration multi-channel seismic (MCS) reflection profiles having a total length of 185 km over the Mona Canyon study area (Fig. 5). The survey employed a 20 airgun array, yielding a total source volume of 8470 cubic inches at 2000 psi. The shot repetition rate was 30 seconds creating an average shot spacing of 77.27 m while maintaining an average ship speed of 5 knots. The towed streamer consisted of 160 channels having a group spacing of 25 m, creating a total distance of 4 km between the near and far channels. The source-to-near channel offset was 187.5 m.

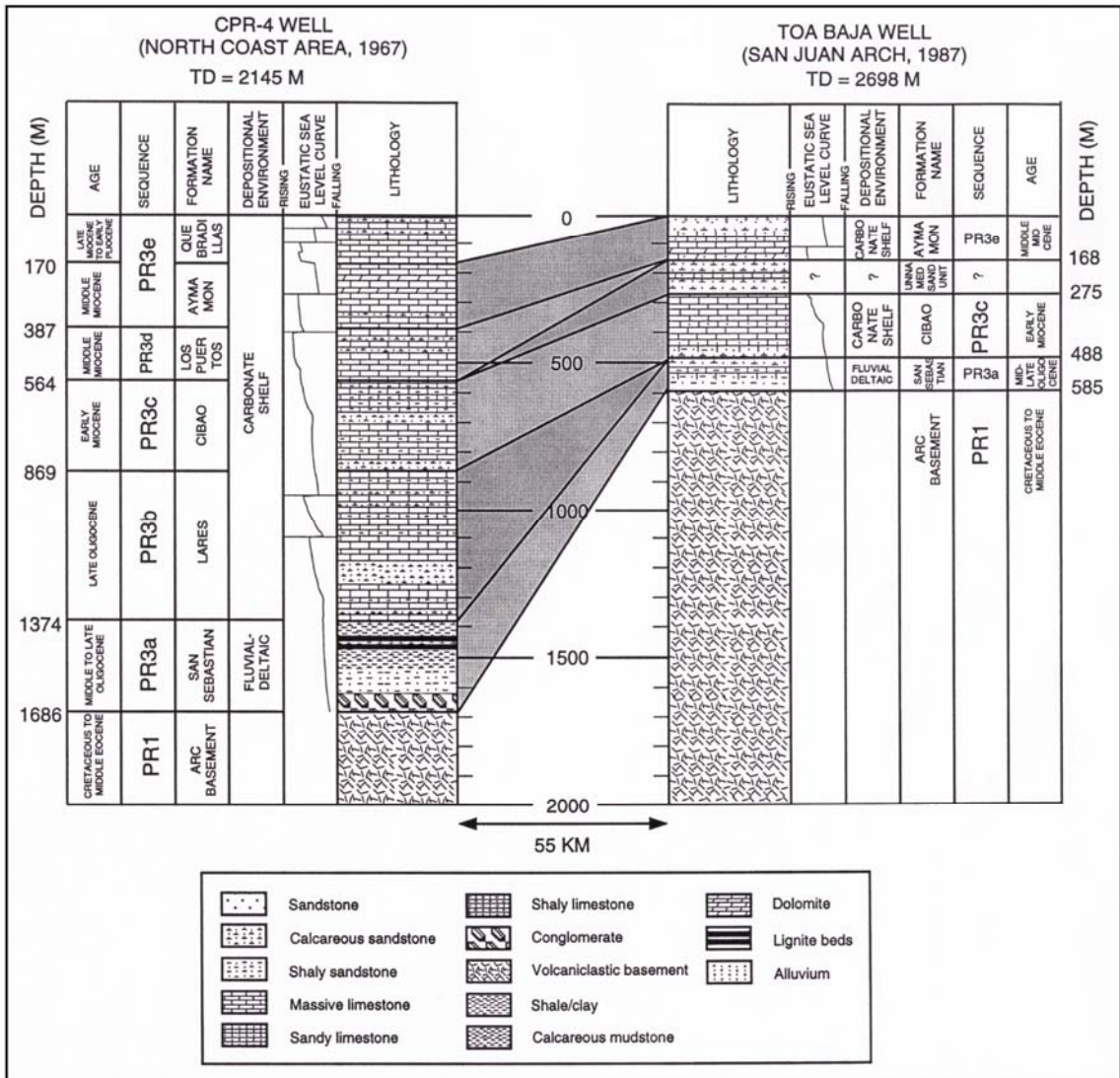
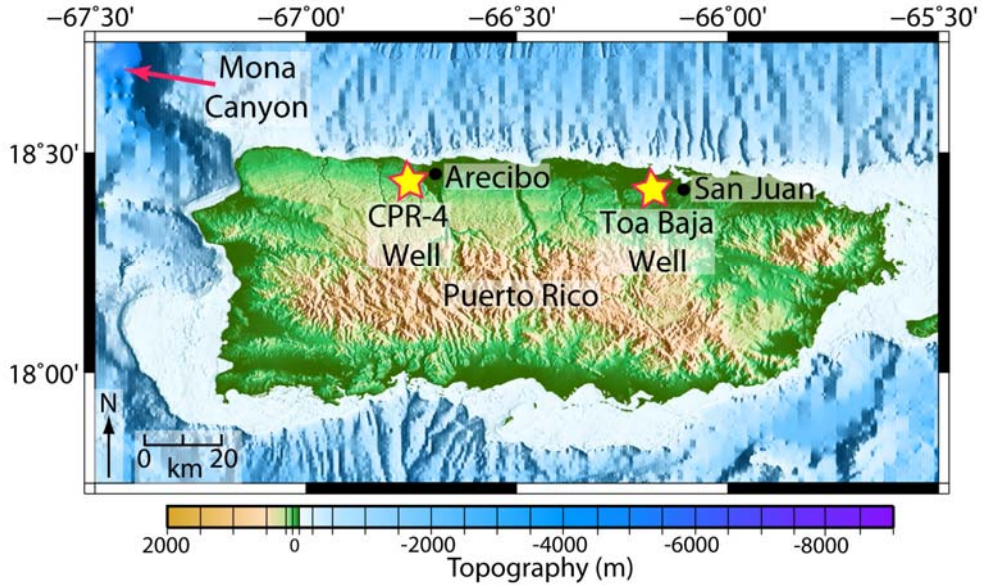
The three EW9501 MCS lines over the Mona Canyon were processed in July, 2006 at the University of Texas at Austin Institute for Geophysics (UTIG) using Paradigm's Focus seismic processing software. Each line utilized the following processing sequence: 1) convert data from SEG-Y format, 2) edit data of missing and noisy shots, 3) define acquisition geometry, 4) correct for spherical divergence, 5) apply single 100 ms gap deconvolution operator, 6) cmp sort and brutestack, 7) perform velocity analysis on every 200 common mid-points (CMPs), 8) apply normal moveout, 9) final stack using stacking velocities, 10) stolt migration using water velocity (1500 m/s), 11) apply time variant bandpass filter (0-4-80-120 Hz), 12) mute water column, and 13) add 500 ms automated gain control (AGC). The final processed data was output to SEG-Y format and imported into Halliburton's Landmark Seisworks software at UTIG in July, 2006 where jpegs were generated for interpretation in Adobe Illustrator.

Interpretation of Single- and Multi-Channel Seismic Reflection Data

The seismic reflection profiles are interpreted stratigraphically according to the three megasequences defined by van Gestel et al. (1999) in the area around the Mona Canyon. These three megasequences are based on the findings of two wells drilled on the north coast of Puerto Rico (Fig. 6); (van Gestel et al., 1999). The stratigraphic-seismic reflection correlations are also matched with MCS line interpretations of Western Geophysical (1974). The area around the Mona Block and north of the Bowin Fault Zone (BFZ) was also assumed to consist of an underlying Late Cretaceous to Middle Eocene blueschist terrane as defined by Perfit et al. (1980) and Heezen et al. (1985), which is similar to the blueschist terrane mapped on the Samana Peninsula of northeast Hispaniola by Joyce (1991). Minor units, including clastic fill, mass wasting deposits, and draped sedimentary cover are also present in the study area. Seismic stratigraphic indicators are defined by the following (Fig. 7):

- 1) Megasequence PR1 is defined by undulating, discontinuous reflectors that cannot be traced for more than a few kilometers and have few internal structures. These reflectors are interpreted to correspond to the Late Cretaceous to Middle Eocene calc-alkaline Greater Antilles island arc volcanic basement rocks that exhibit zeolite to minor greenschist facies metamorphism (Figs. 6 and 7). PR1 also includes arc-derived detritus and pyroclastic debris forming tuff, volcanic sandstone, mudstone, and claystone (van Gestel et al., 1999). The boundary between PR1 and the overlying PR2, where present, or PR3 is a section of strong impedance contrasts evidenced by several, usually three strong positive and negative amplitude reflectors. A green color denotes PR1 in the interpretations of the seismic reflection profiles.

Fig. 6. Stratigraphic columns and correlation of well logs from the CPR-4 well drilled near Arecibo (Briggs, 1961) and the Toa Baja well drilled near San Juan (Gonzalez and Ruiz, 1991). Modified from van Gestel et al. (1999). Note index map at top; yellow stars indicate exact location of wells. Index map generated using NOAA NGDC multibeam bathymetry data. Illumination is from the west. Columns in well logs include age, sequence and formation name, depositional environment, and eustatic sea level curves modified from Haq et al. (1987).



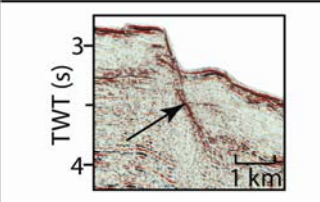
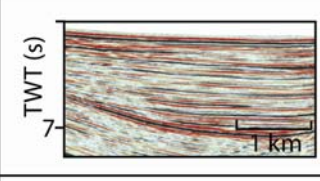
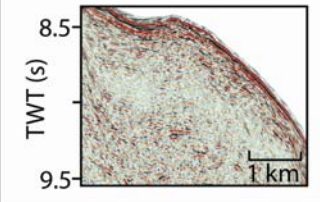
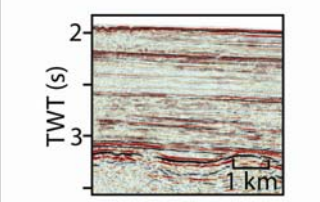
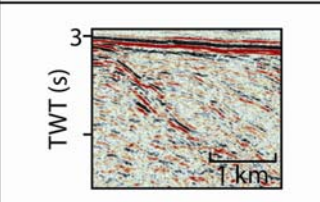
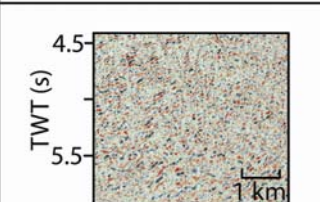
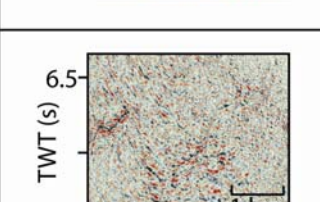
Seismic Facies	Principal Internal Reflector Characteristics	Interpretation	Age
	Break in reflectors, dipping reflectors	Fault	Late Cretaceous to Recent
	Flat-lying, continuous reflectors of varying amplitude, located in basins and other low-lying areas	Ponded turbidites, clastic basin fill, draped sedimentary cover	Late Cretaceous to Recent
	Hummocky, chaotic, low amplitude reflectors	Mass wasting deposits (undifferentiated slumps, slides, flows, avalanches)	Late Cretaceous to Recent
	Straight, parallel, continuous reflectors of varying amplitude	Megasequence PR3 - Puerto Rico-Virgin Islands Carbonate Platform	Middle Oligocene to Late Miocene/ Early Pliocene
	Parallel, semi-continuous reflectors of varying amplitude; frequently exhibit onlapping (diverging reflectors) and mounding appearance	Megasequence PR2 - Marine siliciclastic unit limited to area between north Puerto Rico forearc basin and outer-arc ridge	Late Eocene
	Undulating, discontinuous reflectors of varying amplitude that cannot be traced for more than a few kilometers, few internal structures	Megasequence PR1 - Island-arc volcanic and volcanoclastic basement rocks that exhibit minor zeolite to greenschist facies metamorphism	Late Cretaceous to Middle Eocene
	Undulating, discontinuous reflectors of varying amplitude that cannot be traced for more than a few kilometers, few internal structures	Blueschist facies calc-silicate schist and marble, similar to terrane along Samana Peninsula of northeast Hispaniola	Late Cretaceous to Middle Eocene

Fig. 7. Reflector characteristics used in SCS and MCS interpretation. Figure organized from oldest sequence at the bottom to youngest sequence at the top.

2) Megasequence PR2 is defined by relatively parallel, semi-continuous reflectors that frequently exhibit onlapping and a mounding appearance. Clastic wedges and distal fans often exhibit this characteristic appearance in seismic reflection data. This sequence of reflectors is interpreted to be a Late Eocene marine siliciclastic unit that is limited to the forearc basin between northern Puerto Rico and the outer-arc ridge (Fig. 7). It is composed mostly of reworked volcanic-arc material eroded from the central, subaerial block of Puerto Rico, and transported in northwest-trending depositional environments into the forearc basin by fluvial processes (Dolan et al., 1991; van Gestel et al., 1999). This sequence was not found in either of the two wells drilled on the north coast of Puerto Rico (Fig. 6). Western Geophysical (1974) also did not identify PR2 to be present beneath the PRVI carbonate platform, PR3, in their MCS lines in the Mona Passage, or on the west side of the Mona Canyon. This is explained by a pinching-out of the sequence and the presence of large normal faults in the island-arc basement rocks off the north coast of Puerto Rico (Larue, 1991). The boundary between PR2, where present, and the overlying PR3 sequence consists of a strong impedance contrast generating several positive and negative amplitude reflectors that have an undulating appearance and are traced on all profiles in the Mona Canyon study area. A purple color denotes PR2 in the interpretations of the seismic reflection profiles.

3) Megasequence PR3 is defined by straight, parallel, continuous reflectors. This sequence is correlated with the Middle Oligocene to Late Miocene/Early Pliocene PRVI carbonate platform, and can be subdivided into individual sequences using major continuous and correlatable reflectors (Figs. 6 and 7). For ease of structural interpretation, PR3 has only been subdivided when comparing the seismic reflectors and

stratigraphy of the PRVI carbonate platform on the different sides of the Mona Canyon to help determine the canyon's age (see Results and Interpretation section). PR3a is the Middle to Late Oligocene San Sebastian Formation, which is a northward prograding siliciclastic unit that filled in low areas above the undulating arc basement, PR1, and forearc basin unit, PR2. This unit begins as a basal conglomerate and is transitional into sandstone, becoming more calcareous towards the top. PR3b-3e are the Late Oligocene Lares, Early Miocene Cibao, Middle Miocene Los Puertos, and Middle Miocene to Early Pliocene Aymamon and Quebradillas Formations, respectively (Fig. 6). These formations consist mainly of shallow, 100-200 m maximum depositional water depths, clear water limestone, representing a period of depositional tectonic quiescence. Intermittent chalk, marl, and some sand beds are also present in this megasequence (Fig. 6); (Larue, 1991; van Gestel et al., 1999). A red color denotes PR3 in the interpretations of the seismic reflection profiles.

4) The blueschist facies rocks in the Mona Block region exhibit thrust faulting plainly visible in the seismic data, but lack any other significant reflector characteristics that help to distinguish this unit from PR1 (Fig. 7). A blue color denotes the blueschist terrane in the interpretations of the seismic reflection profiles.

5) In many areas between the present shelf-slope break and the Puerto Rico trench, the blueschist facies rocks and other island arc volcanic and volcanoclastic rocks are observed to be capped by a draped pelagic sedimentary cover. This sedimentary unit displays very low amplitude, flat lying reflectors that cover the underlying rocks (Grindlay et al., 2005). Flat lying reflectors along the axis of the Mona Canyon are interpreted to be clastic basin-fill sediments, which are likely dominantly ponded

turbidite deposits (Fig. 7); (Fox and Heezen, 1975; Heezen et al., 1985). The draped sedimentary cover and clastic basin-fill deposits are denoted with a yellow color in the interpretations of the seismic reflection profiles. Apparent slide and talus blocks and chaotic, hummocky reflectors are used to identify potential mass wasting features (Fig. 7). An orange color denotes mass wasting deposits in the interpretations of the seismic reflection profiles.

The profiles are interpreted structurally by locating and analyzing reflector offsets and dipping reflectors to identify faults (Fig. 7). Black lines denote faults, with half-arrows indicating directions of relative displacement, in the interpretations of the seismic reflection profiles. Profiles with and without interpreted and labeled stratigraphic horizons, potential faults, and mass wasting features are presented in the following sections. Midland Valley's 2DMove v.5.0 software was used to view the seismic sections in three dimensions in order to maintain consistency between the interpretations. Fault tip line surface expression locations and surficial lithologic unit contacts were then projected onto a bathymetry-trackline map using shot point record locations from the seismic navigation records on both planar and profile views. Faults and contacts were then interpolated between reasonably close, less than 10 km spacing, tracklines on the bathymetric map in order to map lithologic unit contacts, active faults at the seafloor level, and submarine mass wasting features in the study area.

Earthquake Data

Earthquake seismicity data recorded from 1973-2007 were downloaded from the online USGS National Earthquake Information Center (NEIC), which combines data from several sources including the Puerto Rico Seismic Network (PRSN). The locations of additional significant historical earthquakes are catalogued by Pacheo and Sykes (1992). The Harvard University Centroid-Moment Tensor Catalog (CMT) provides calculated focal mechanism solutions (FMS) from earthquakes that have occurred in the study area from 1976-2007. These focal mechanism data are supplemented with moment tensor data from Dolan and Wald (1998) and Doser et al. (2005) to produce additional FMS that are overlain onto the other marine geophysical data.

In this study, FMS, earthquake locations, and magnitudes are used to examine the relationship between the distribution and type of events and faults identified in the marine geophysical data. Local and regional seismic networks have foci of spatially and temporally concentrated strings of shallow earthquakes having focal depths less than 20 km in the region of the Mona Canyon that may be situated along fault planes. These relationships aid in mapping the attributes of significant faults identified in the marine geophysical data, including their locations, lengths, and magnitude of the displacements.

RESULTS AND INTERPRETATION OF MARINE GEOPHYSICAL DATA

The marine geophysical data described above is used to evaluate the morphology, structure, and tectonic evolution of the Mona Canyon. This study uses the multibeam bathymetry, sidescan sonar imagery, single- and multi-channel seismic reflection profiles, and earthquake foci to map lithologic units, active faults having seafloor expressions, and major areas of slope instability. Detailed evaluation of this data also provides evidence for proposing an approximate age, timing of events, and potential causes for the formation of the Mona Canyon.

Morphology and Structure

In plan view, the Mona Canyon has a “Z” shape, and is 140 km-long, 20-30 km-wide, and 2-3.5 km-deep relative to the surrounding seafloor. It has a maximum water depth of over 7.8 km in the northern Mona Canyon where it is transitional into the Puerto Rico trench (Fig. 5). The morphology described in detail below indicates the Mona Canyon is an atypical submarine canyon, as compared to erosional submarine canyons, such as the Hudson and Monterey submarine canyons on the eastern and western margins of the United States, respectively (Shepard, 1981). The Mona Canyon, Mona Block, sinistral Bowin, Bunce, and East Septentrional fault zones, and the normal or normal-oblique Mona Canyon fault all have clear bathymetric expressions (Fig. 5). On the basis of trend and along-axis gradient, the Mona Canyon can be separated into three domains for ease in structural interpretation: a southern, central, and northern Mona Canyon domain, the latter of which includes the Mona Block. The morphology and structure of each domain are described below:

Southern Mona Canyon

Immediately off the northwest coast of Aguadilla, Puerto Rico is the northwest-trending southern Mona Canyon. The southern domain exhibits an upside-down v-shape, having a shallower, more poorly defined, western side (Fig. 5). Isla Desecheo marks the highest point along the Desecheo Ridge, which is a narrow, less than 5 km-wide, northwest-trending ridge that extends off the west coast of Punta Higuero, Puerto Rico, and defines the south wall of the southern Mona Canyon. Another narrow, less than 5 km-wide, northwest-trending ridge, here informally referred to as Agujereada Ridge for its close proximity to Punta Agujereada at the northwest tip of Puerto Rico, is the north wall of the southern Mona Canyon (Fig. 5).

The southern region is approximately 40 km-long, an average of 23 km-wide, 0-2.5 km-deep relative to the surrounding seafloor (3.5 km maximum water depth), and has an along-axis gradient of 105 m/km (Fig. 8). This along-axis gradient is in stark contrast to the average 4°, and maximum 8° dip of the northern Puerto Rico margin (van Gestel et al., 1998, 1999). The across-axis bathymetric profiles show the southern Mona Canyon is highly asymmetrical, with the Agujereada Ridge north wall being the steeper side (Fig. 8). The north wall has a 25° average slope that approaches 48° in areas, while the south wall has a less than 10° slope on average. The southern Mona Canyon also has a u-shaped across-axis profile. This morphology is in contrast to more typical submarine canyons, which have symmetric, v-shape profiles, and are typically less than 10 km wide (Shepard, 1981).

EW9605 SCS Line 32 is a northeast-trending section that crosses perpendicular to the southern Mona Canyon approximately 20 km northwest of Aguadilla (Fig. 9). This

Fig. 8. Across-axis bathymetric profiles 1-9 and along-axis composite bathymetric profile A-B-C-D. Profiles are across the southern, central, and northern Mona Canyon. See index map at top left for locations of profiles; dashed lines indicate boundaries for domains; magenta – southern Mona Canyon, black – central Mona Canyon, red – northern Mona Canyon and Mona Block domains. Arrow denotes axis of canyon on across-axis profiles. Arrows on along-axis profile denote location of turns in profile. In along-axis composite profile, the apparent mass wasting deposit shown is not used in calculating the gradients of the southern and central Mona Canyon. SMC – Southern Mona Canyon, CMC – Central Mona Canyon, NMC – Northern Mona Canyon, MB – Mona Block, Pt. A. – Pt. Agujereada, Pt. H. – Pt. Higuero.

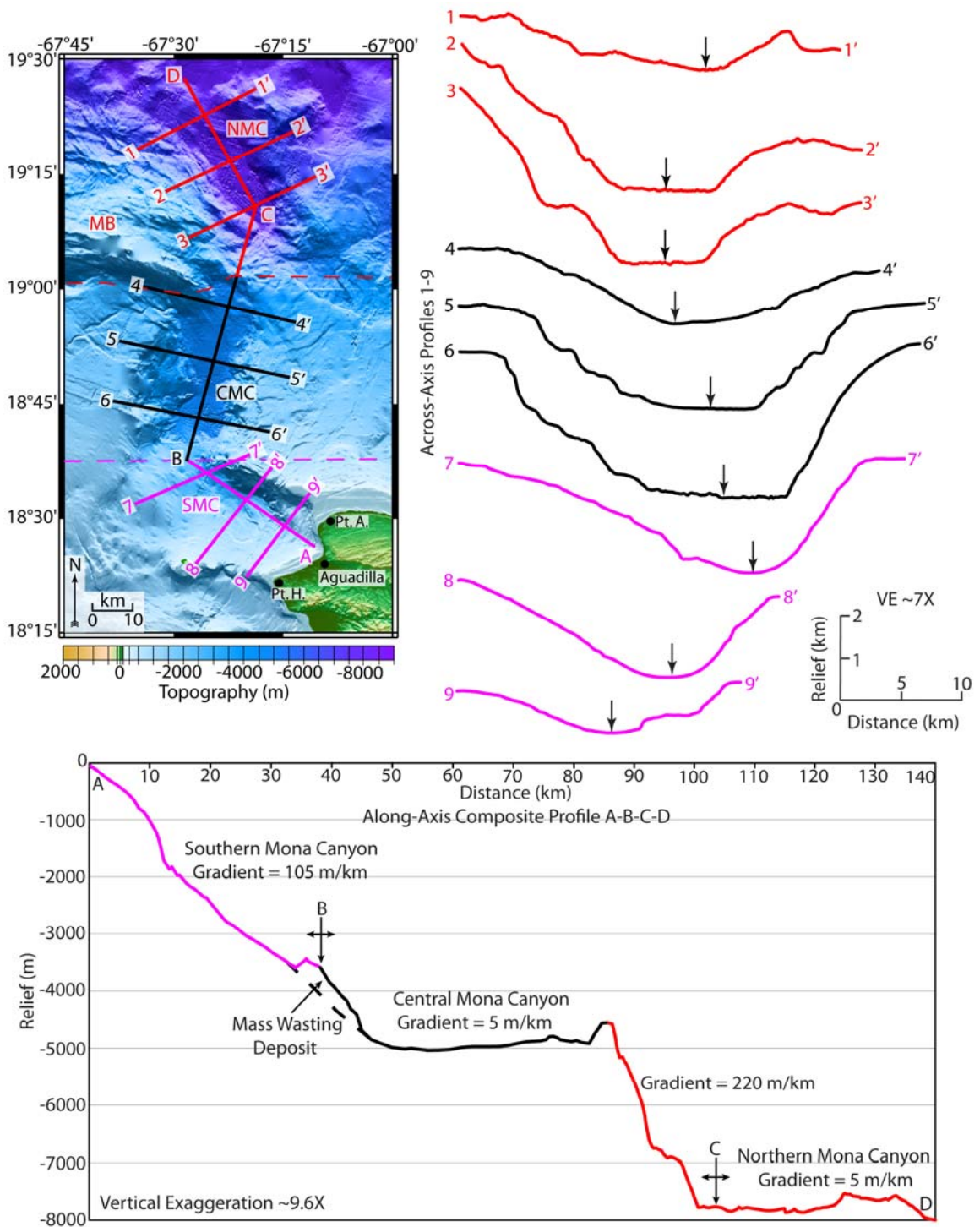
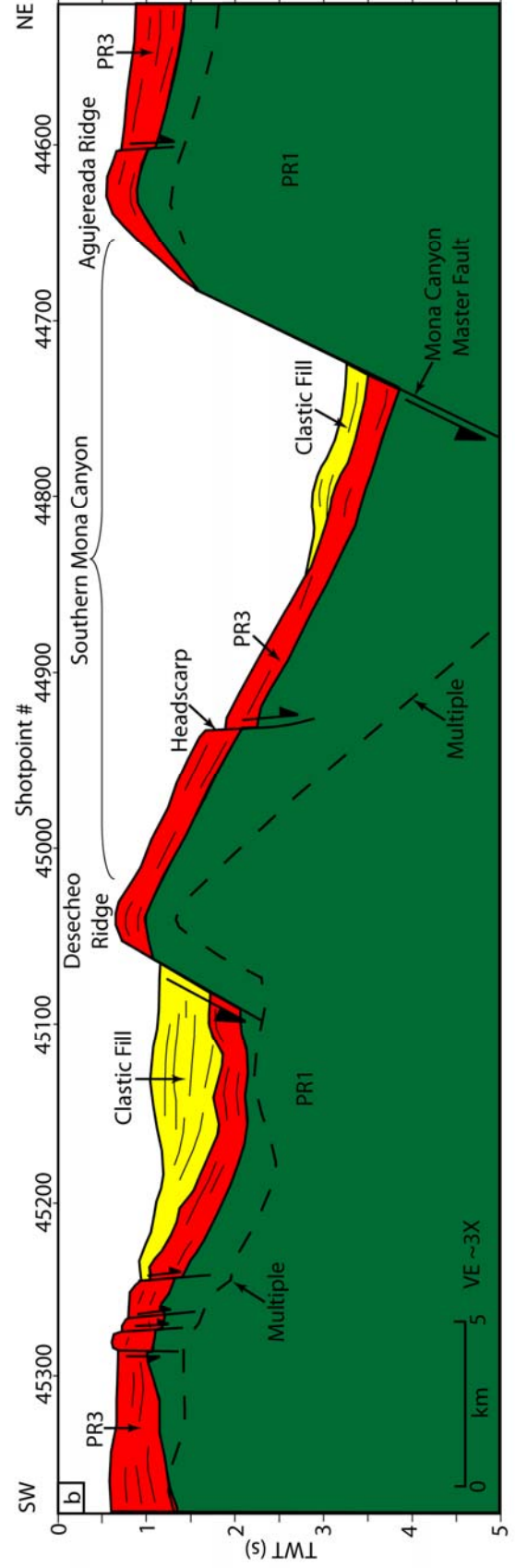
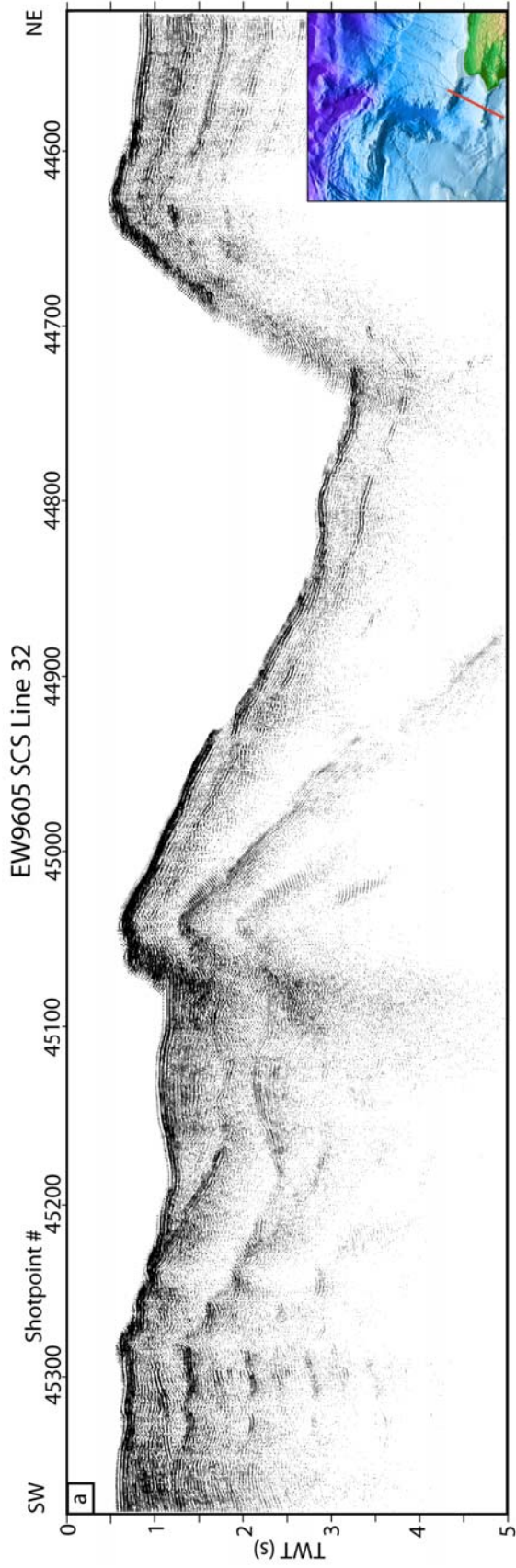


Fig. 9. EW9605 SCS Line 32. Southern Mona Canyon; see index map at bottom right of (a) for exact location. a. Processed data. b. Line drawing interpretation of processed data. Dashed line is multiple seafloor reflection. Vertical exaggeration is approximately 3X. Green unit represents PR1, red unit represents PR3, yellow unit represents clastic fill.

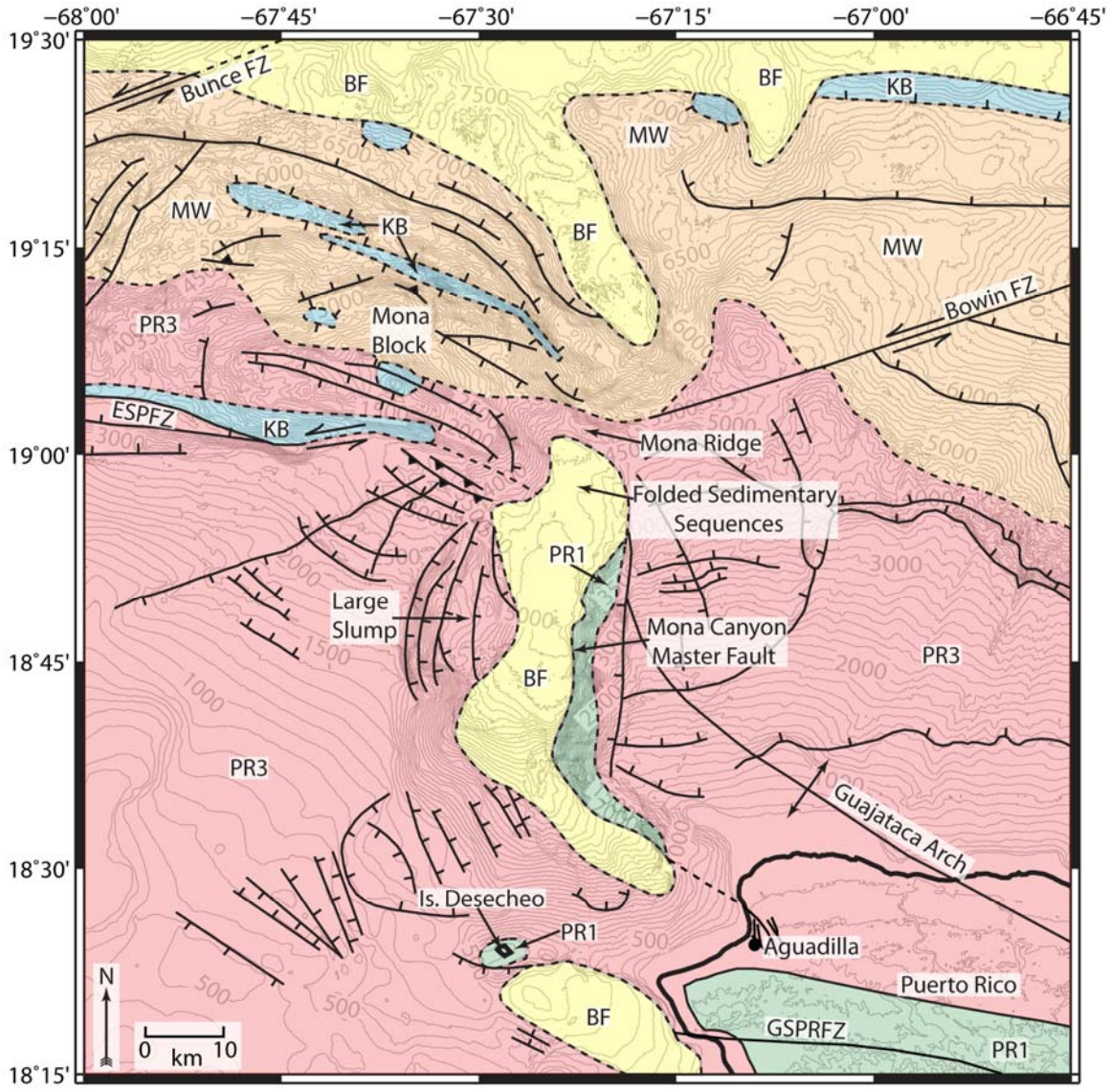


seismic line shows that the northwest-trending, southwest-dipping normal or normal-oblique Mona Canyon master fault bounding Agujereada Ridge controls the asymmetric nature of the southern Mona Canyon. The master fault scarp exposes the underlying PR1 rocks along the north wall of the canyon (Fig. 10). One secondary antithetic fault on the southwest side creates a half-graben structure (Fig. 9). This antithetic fault also creates a 200 m-high headscarp along the southwest wall of the southern Mona Canyon at approximately 1200 m water depth. The seismic section shows the PRVI carbonate platform, PR3, immediately caps PR1 rocks. The siliciclastic forearc basin unit PR2 appears to be missing in the southern domain of the Mona Canyon. Using an interval velocity of 1850 m/s as determined from the velocity analysis of MCS CMP data, an approximately 200 m-thick section of more recent clastic basin-fill sediments cover the axis of the southern Mona Canyon. To the southwest of Desecheo Ridge is another half-graben filled with what are interpreted to be an approximately 700 m-thick sequence of clastic basin-fill sediments that overly PR3 carbonate rocks.

Central Mona Canyon

The north-trending central Mona Canyon has the most apparent bathymetric expression in the study area (Figs. 5 and 8). The central domain is approximately 50 km-long, an average of 27 km-wide, 2-3.5 km-deep relative to the surrounding seafloor (5 km maximum water depth), and has an along-axis gradient of 5 m/km (Fig. 8). The across-axis bathymetric profiles indicate that the central Mona Canyon is slightly more symmetrical than the southern region, having a 30° average sloped east wall that approaches 50° locally, and a 10° sloped west wall on average (Fig. 8). Another narrow,

Fig. 10. Generalized geologic map of Mona Canyon study area. Map illustrates major faults and lithologic units at the seafloor level. Map generated by projecting fault tip lines and lithologic unit contacts to the surface from the seismic reflection sections using shot point record locations, and combining this data with evidence in the multibeam bathymetry and sidescan sonar imagery. Dredges shown in Fig. 5 are used for ground-truth. Note key at bottom of map for colors and symbols used. See Fig. 5 and text for description of data used to make map. Basemap is same bathymetric data set as in Figs. 5 and 8, and has a contour interval of 100 m. ESPFZ – East Septentrional Fault Zone, GSPRFZ – Great Southern Puerto Rico Fault Zone.



- | | |
|--|--|
| <ul style="list-style-type: none"> BF Clastic basin-fill sediments - includes turbidites and other draped sedimentary cover MW Mass wasting deposits (undifferentiated) PR3 Middle Oligocene to Late Miocene/ Early Pliocene Puerto Rico-Virgin Islands carbonate platform (mostly limestone) PR1 Late Cretaceous to Middle Eocene zeolite to greenschist facies calc-alkaline island arc volcanic rocks and volcanoclastics KB Late Cretaceous to Middle Eocene blueschist terrane - calcsilicate-schist and marble | <ul style="list-style-type: none"> Lithologic contact - solid where known, dashed where inferred Guajataca Arch axis Normal fault - bar on hanging wall block, solid where exposed, dashed where concealed Reverse fault - teeth on hanging wall Strike-slip fault - half-arrows show direction of relative displacement |
|--|--|

less than 5 km-wide, northwest-trending saddle that extends off the eastern edge of the Mona Block, informally referred to as Mona Ridge, defines the north end of the central Mona Canyon (Figs. 8 and 10).

East-trending EW9501 MCS Line 1289 crosses approximately perpendicular to the central Mona Canyon (Fig. 11). This section displays the north-trending, west-dipping normal or normal-oblique Mona Canyon master fault on the east side of the canyon controls the half-graben structure of the central domain (Fig. 11). This fault exhibits a sense of vertical component of dip separation of up to 3.5 km, and exposes the underlying PR1 rocks along the scarp face. EW9501 MCS Line 1289 shows the Mona Canyon master fault has listric geometry with an upper segment dip of 45° that shallows to approximately 25° at depth. However, it does not appear the footwall of the half-graben (Guajataca Arch) has been uplifted higher than the hanging wall during inferred extension. The footwall is in fact 500 m, or approximately 375 m, lower than the hanging wall (Fig. 11).

EW9501 MCS Line 1289 provides evidence that north-trending, east-dipping antithetic faults having individual vertical components of dip separation averaging less than 1 km bound several rider blocks on the shallower west side of the central Mona Canyon half-graben. The hanging wall dips more shallowly than the footwall at 9.5° . Flat-lying reflectors along the axis of the canyon are interpreted to be an approximately 600 m-thick sequence of syndepositional clastic graben fill sediments.

EW9501 MCS Line 1289 provides evidence that PR3 is significantly thicker and more constant and seismically homogeneous on the west side of the canyon than it is on the east, averaging 1650 m- and 750 m-thick, respectively. A more detailed view of the

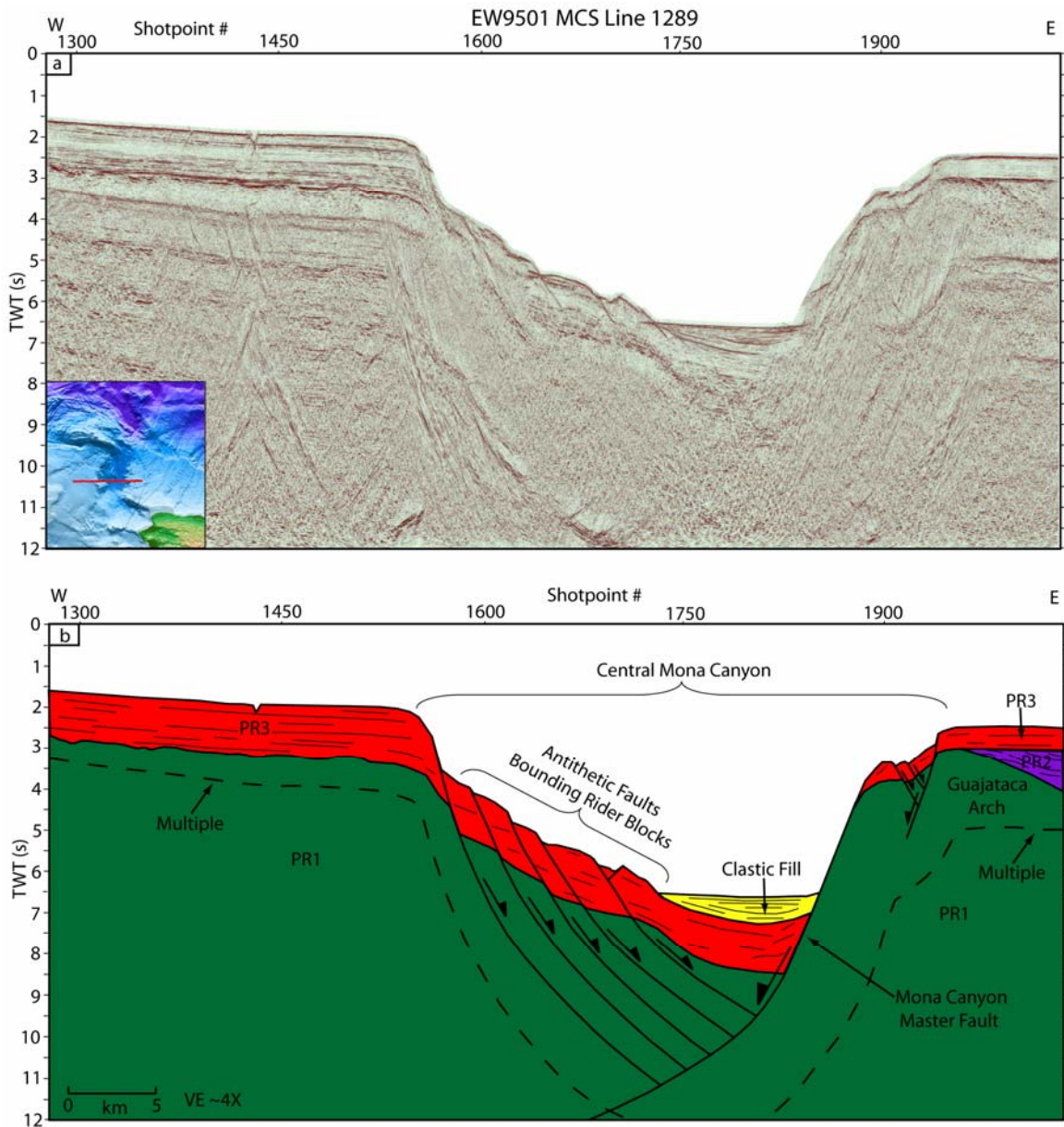


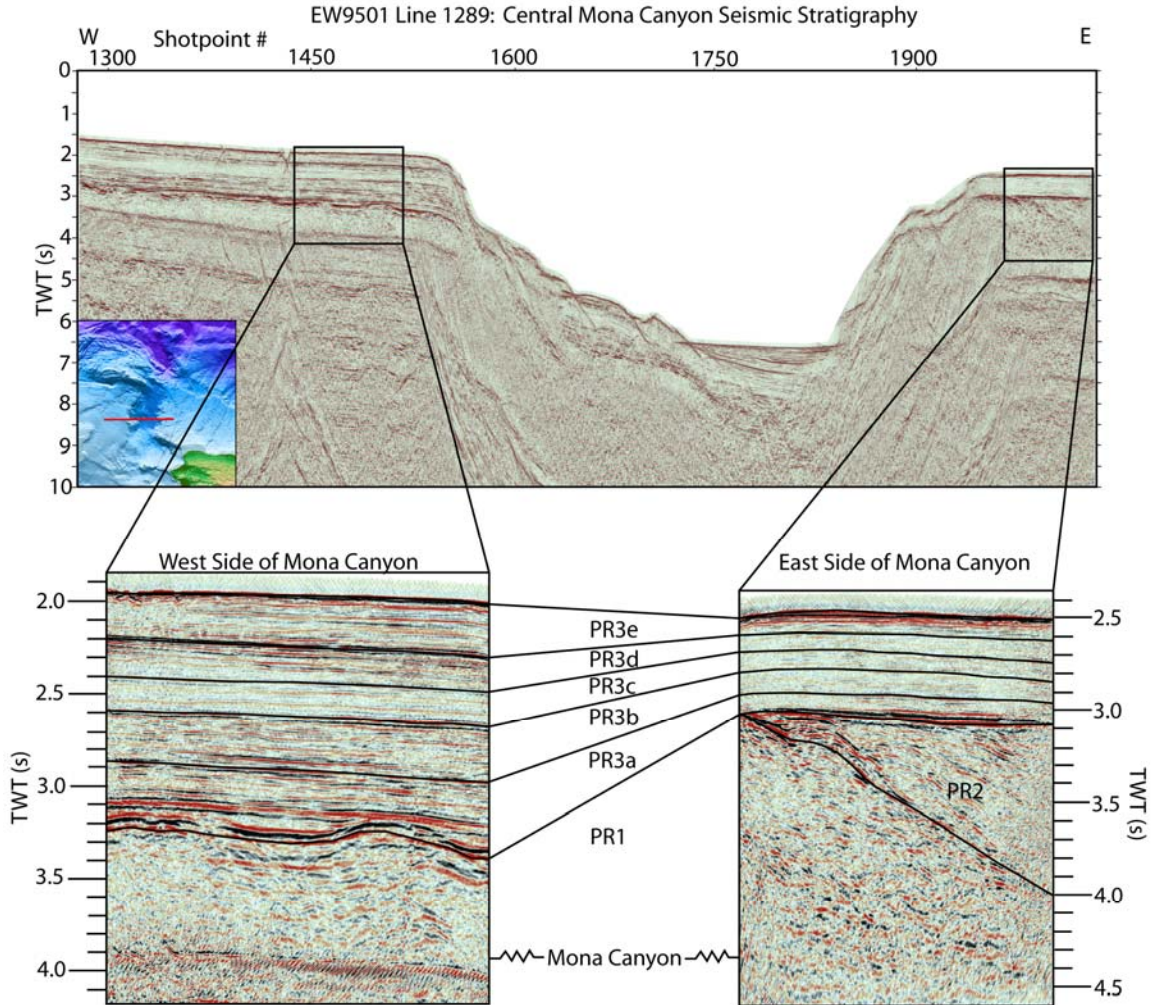
Fig. 11. EW9501 MCS Line 1289. Central Mona Canyon; see index map at bottom left for exact location of section. a. Processed data. b. Line drawing interpretation of processed data. Dashed line is multiple seafloor reflection. Vertical exaggeration is approximately 3X. Green unit represents PR1, purple unit represents PR2, red unit represents PR3, yellow unit represents clastic fill.

seismic stratigraphy from opposite sides of the Mona Canyon using this high-resolution seismic line shows that overall, the PR3 shallow water carbonate platform is nearly 1000 m thicker on the west side of Mona Canyon compared to the east side, using an interval velocity of 2850 m/s from the velocity analysis of MCS CMP data (Fig. 12). The data indicate that all the subunits of the PR3 carbonate rocks are present on both sides of the Mona Canyon. However, these units appear to be much thinner on the footwall as compared to the hanging wall (Fig. 12). PR2 is also not present on the hanging wall.

Northern Mona Canyon and Mona Block

The less than 5 km-wide, east-southeast-trending ridge centered at $-67^{\circ}22'W$ x $19^{\circ}2'N$ informally referred to here as Mona Ridge marks the beginning of a steep, 220 m/km slope that is transitional into the deepest and northernmost region of the Mona Canyon (Figs. 5, 8, and 10). The northern Mona Canyon is approximately 50 km-long, an average of 17 km-wide, up to 2 km-deep relative to the surrounding seafloor (7.8 km maximum water depth). It has an along-axis gradient of 5 m/km (Fig. 8). The west wall of the northern domain has an average slope of 25° and approaches 45° locally, while the east wall has an average slope of 10° . The across-axis bathymetric profiles show how the Mona Block exaggerates the west wall of the northern Mona Canyon, mirroring the asymmetric aspect of the southern and central domains (Fig. 8). To the north of $19^{\circ}26'N$, the Mona Canyon is transitional into the depths of the Puerto Rico trench.

EW9605 SCS Line 25 indicates that the Mona Ridge marks the approximate contact between PR1 volcanic and volcanoclastic rocks and the Late Cretaceous to Middle Eocene blueschist terrane along a down-to-the-south normal fault (Fig. 13). This ridge is

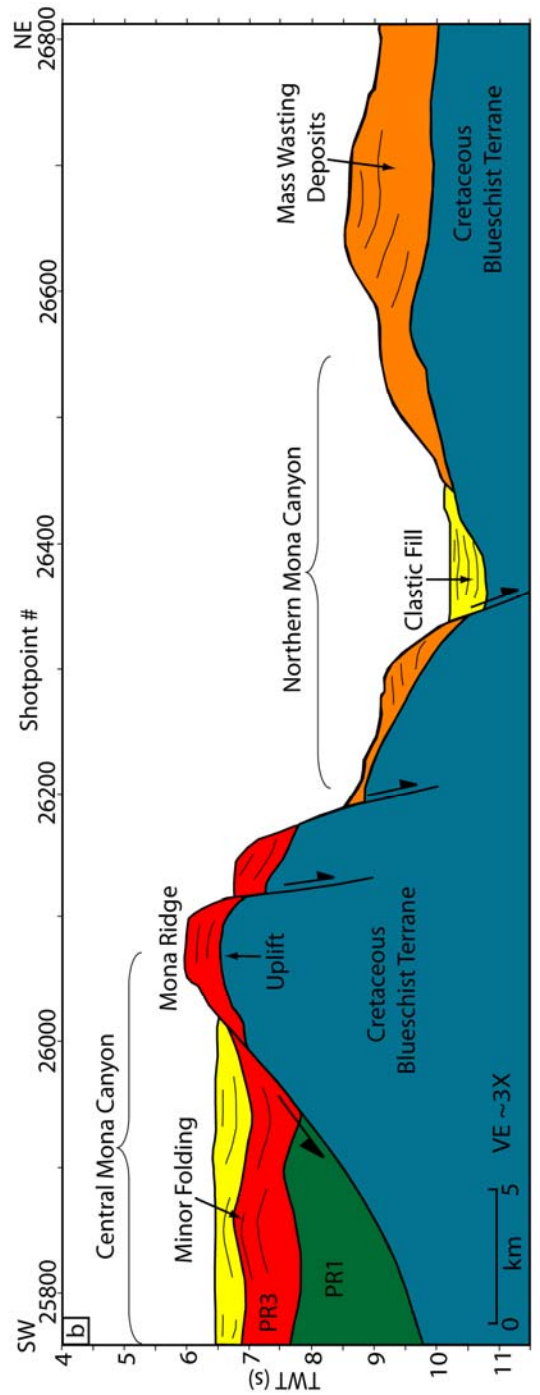
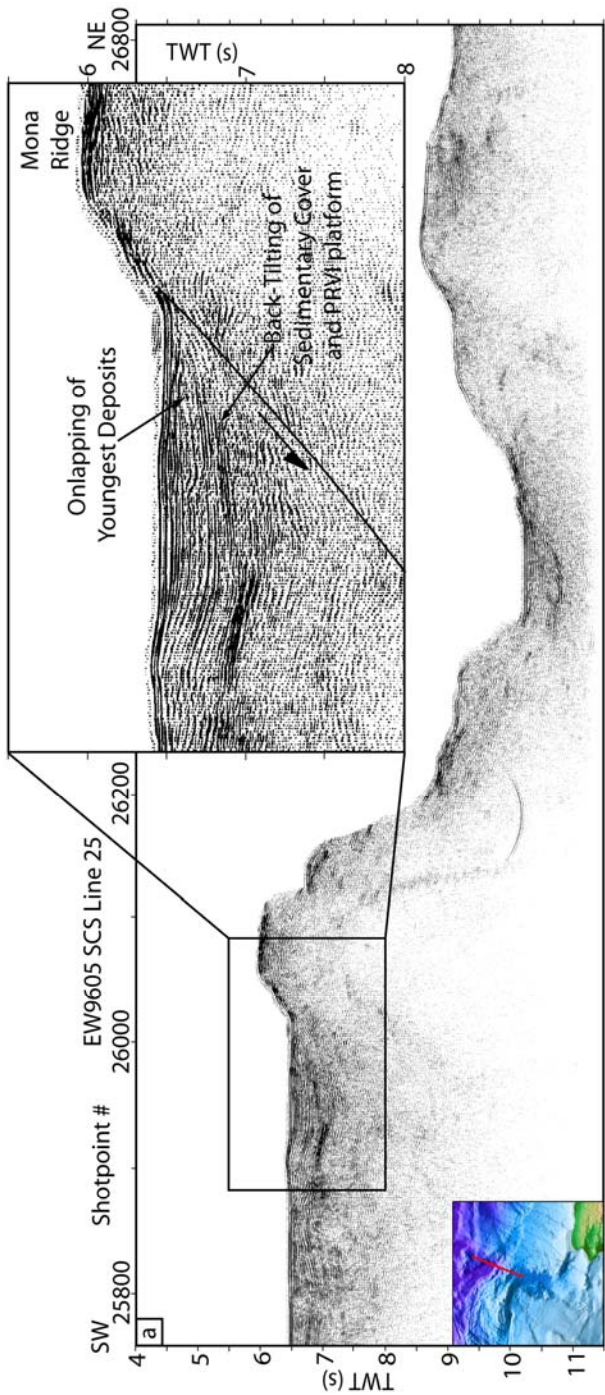


Middle Oligocene to Late Miocene/Early Pliocene Puerto Rico-Virgin Islands Carbonate Platform				
Sequence	Formation Name	Age	Thickness (m)	
			West Side	East Side
PR3a	San Sebastian	Middle to Late Oligocene	513	185
PR3b	Lares	Late Oligocene	371	214
PR3c	Cibao	Early Miocene	285	143
PR3d	Los Puertos	Middle Miocene	285	114
PR3e	Aymamon	Middle Miocene	342	171
	Quebradillas	Late Miocene to Early Pliocene		
		TOTAL	1796	827

**Using an interval velocity of 2850 m/s for PR3

Fig. 12. Detailed view of seismic stratigraphy over central Mona Canyon. Data obtained from EW9501 MCS Line 1289; note line and locations in top image. Line chosen for its high-resolution and its approximately perpendicular orientation to the central Mona Canyon. PR3 depth conversion performed using an interval velocity of 2850 m/s as determined from the velocity analysis of MCS CMP data.

Fig. 13. EW9605 SCS Line 25. Central to Northern Mona Canyon; see index map at bottom left for exact location of section. a. Processed data. b. Line drawing interpretation of processed data. Dashed line is multiple seafloor reflection. Vertical exaggeration is approximately 3X. Green unit represents PR1, red unit represents PR3, blue unit represents blueschist terrane, orange unit represents mass wasting deposits, yellow unit represents clastic fill.



defined as a region of post-Pliocene uplift due to the back-tilting of surficial seismic reflectors interpreted to be sedimentary cover onto the Mona Ridge; only the very youngest (upper 0.2 s, or 185 m) deposits show evidence of onlapping (Fig. 13). This sedimentary unit and the underlying PRVI carbonate platform appear to be folded, providing evidence for NE-SW-directed shortening (Fig. 13). Parallel reflectors capping the Mona Ridge are interpreted to be the northern extent of the PRVI platform (Fig. 10). However, interpreted slumped carbonate blocks are visible in the seismic data along the steep southern slope of the northern Mona Canyon. High-angle, greater than 45°, west and northwest-trending normal faults are evident along this steep slope on the northern side of the Mona Ridge (Fig. 13). The axis of the northern Mona Canyon is covered by approximately 600 m-thick sequences of clastic basin fill. This domain is also fault controlled, with normal displacements on the order of 1.5 km (Fig. 5). The blueschist facies rocks in the northern Mona Canyon are interpreted to be capped by an approximately 1 km-thick sequence of mass wasting deposits (Fig. 13).

EW9501 MCS Line 1290 is perpendicular to MCS Line 1289, and shows an amphitheater-shaped headscarp at approximately 19°N marks the beginning of rollover folding in PR2 and PR3 (Fig. 14). The headscarp and rollover structure are both likely due to normal displacement along the northeast-trending, sub-vertical, sinistral Bowin fault zone (Figs. 5, 10, and 14). This MCS section indicates the northern extent of the carbonate platform along the Bowin fault zone, which is transitional into 1 km-thick sequences of mass wasting deposits that overlie the Cretaceous blueschist terrane in the northern Mona Canyon (refer to Fig. 7). The PRVI carbonate platform is inferred to have subsided from its deposition near sea level to its current position at a maximum water

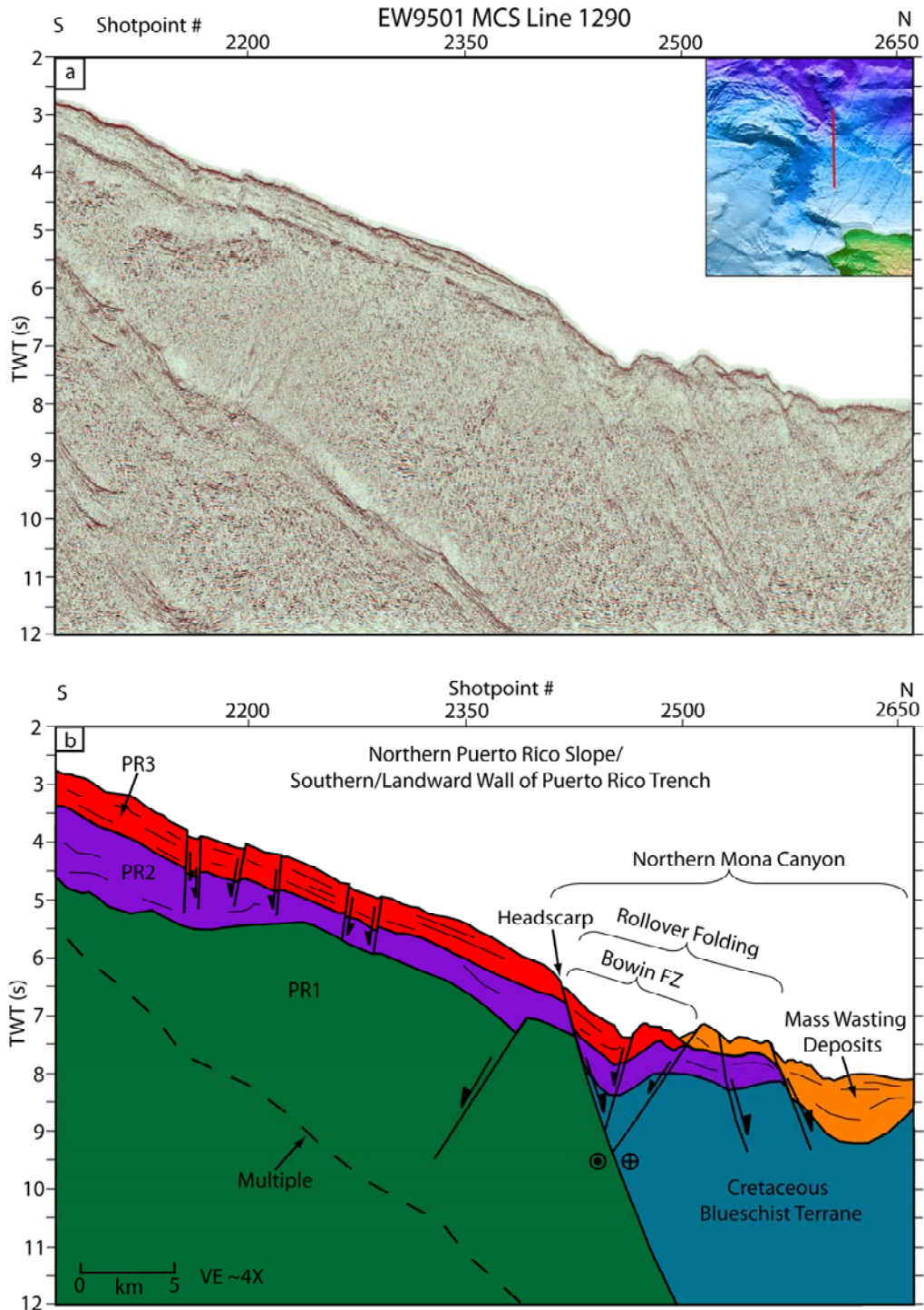


Fig. 14. EW9501 MCS Line 1290. Northern Puerto Rico Slope and Northern Mona Canyon; see index map at top right for exact location of section. a. Processed data. b. Line drawing interpretation of processed data. Dashed line is multiple seafloor reflection. Vertical exaggeration is approximately 4X. Green unit represents PR1, purple unit represents PR2, red unit represents PR3, blue unit represents blueschist terrane, orange unit represents mass wasting deposits.

depth of 4.5 km (Fig. 10). Here, the onlapping and mounding seismic reflector characteristics of the PR2 forearc basin unit are clearly visible beneath the PR3 seismic reflectors. These reflectors are not visible on the west side of Mona Canyon, such as in MCS Lines 1289 and 1291 (Figs. 11 and 15, respectively).

EW9501 MCS Line 1291 indicates that west and northwest-trending, north and northeast-dipping, sub-vertical normal faults have caused extensive mass wasting on the southwest side of the northern Mona Canyon (Fig. 15). The northeast side of the northern Mona Canyon consists of numerous sequences of mass wasting deposits that are up to 1 km thick and overly the metamorphic terrane.

EW9501 MCS Line 1291 shows that the hypothesized region of uplift, the Mona Block, is a 60 km x 40 km high-standing feature that rises up to 7 km above the surrounding seafloor (713 m minimum water depth) (Fig. 15). The Mona Block is bound to the south by the northwest-trending, sub-vertical, sinistral East Septentrional fault zone (ESPFZ) and down-dropped blocks on its steep, 25-45°, north side. These fault blocks are displaced by west- and northwest-trending normal faults having maximum vertical component of dip separations of approximately 1.5 km along the top of the Mona Block (Fig. 15).

Parallel seismic reflectors near the top of the Mona Block in EW9501 MCS Line 1291 and EW9605 SCS Lines 27 and 29 potentially indicate that this region is composed of the carbonate platform, PR3, cap that overlies an uplifted portion of the Cretaceous blueschist terrane (Figs. 15, 16, and 17). The carbonate cap is interpreted to be folded into an anticlinal structure in EW9501 SCS Line 29 (Fig. 17). The northwest-trending, ESPFZ appears to be the sub-vertical fault contact between PR1 and Cretaceous

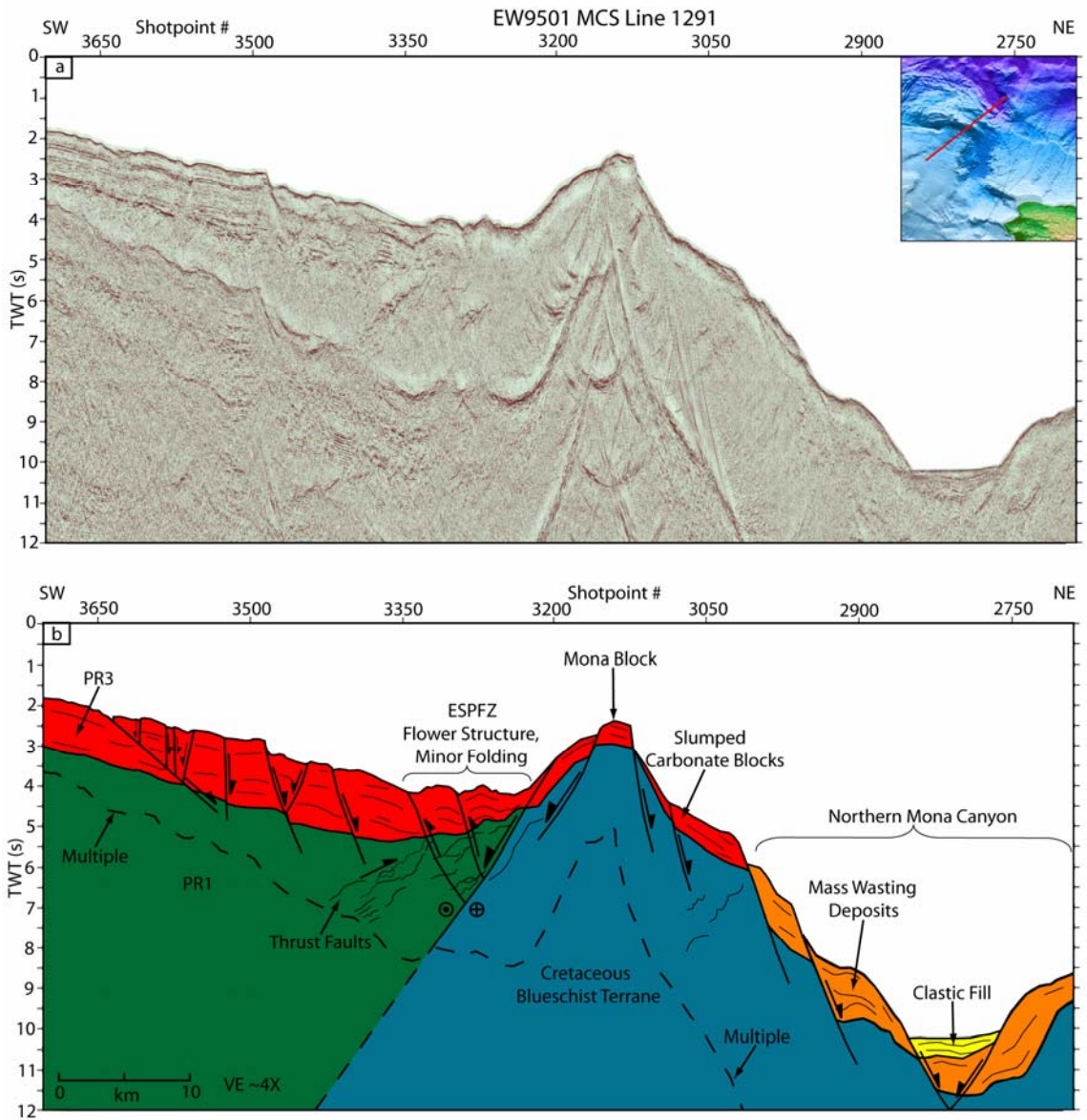


Fig. 15. EW9501 MCS Line 1291. Mona Block and Northern Mona Canyon; see index map at top right for exact location of section. a. Processed data. b. Line drawing interpretation of processed data. Dashed line is multiple seafloor reflection. Vertical exaggeration is approximately 4X. Green unit represents PR1, red unit represents PR3, blue unit represents blueschist terrane, orange unit represents mass wasting deposits, yellow unit represents clastic fill.

Fig. 16. EW9605 SCS Line 27. Mona Block and northern Mona Canyon; see index map at top right for exact location of section. a. Processed data. b. Line drawing interpretation of processed data. Dashed line is multiple seafloor reflection. Vertical exaggeration is approximately 3X. Green unit represents PR1, red unit represents PR3, blue unit represents blueschist terrane, orange unit represents mass wasting deposits, yellow unit represents clastic fill.

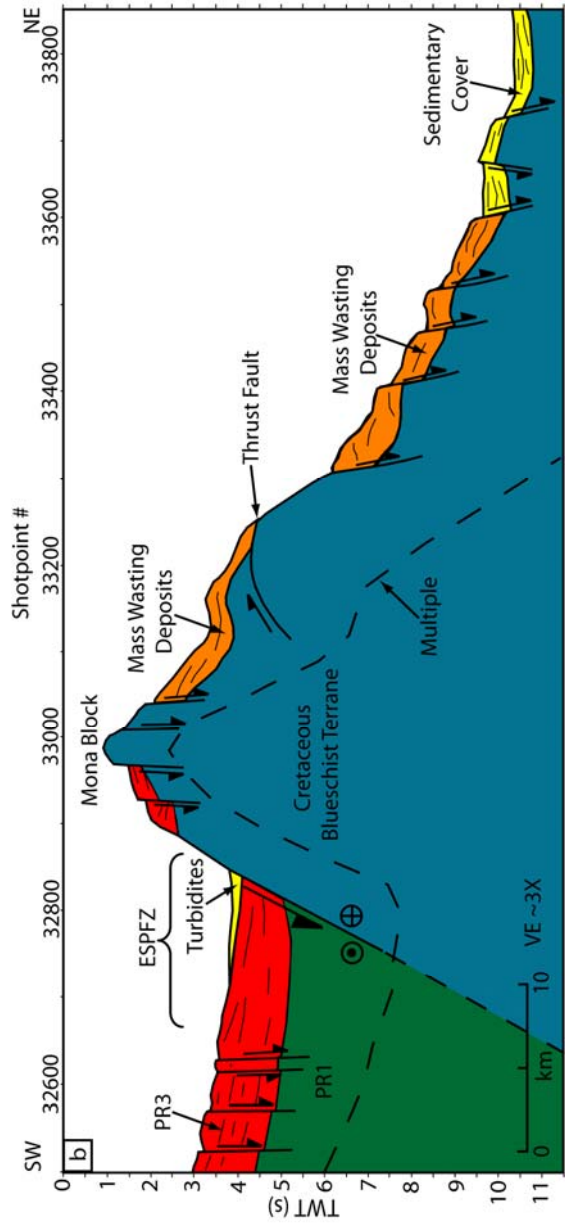
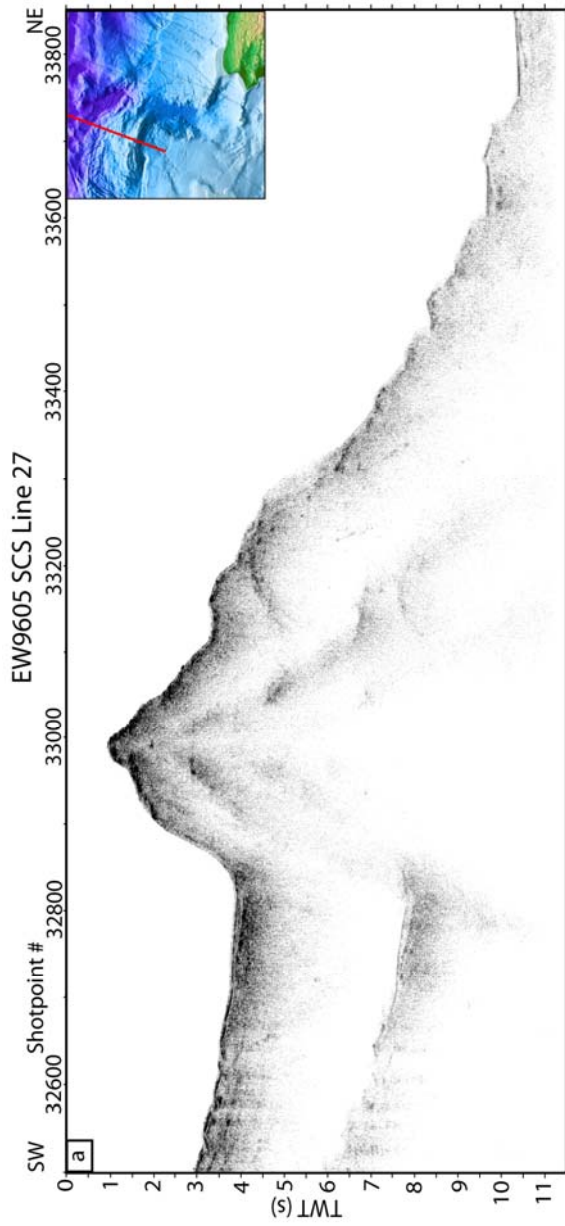
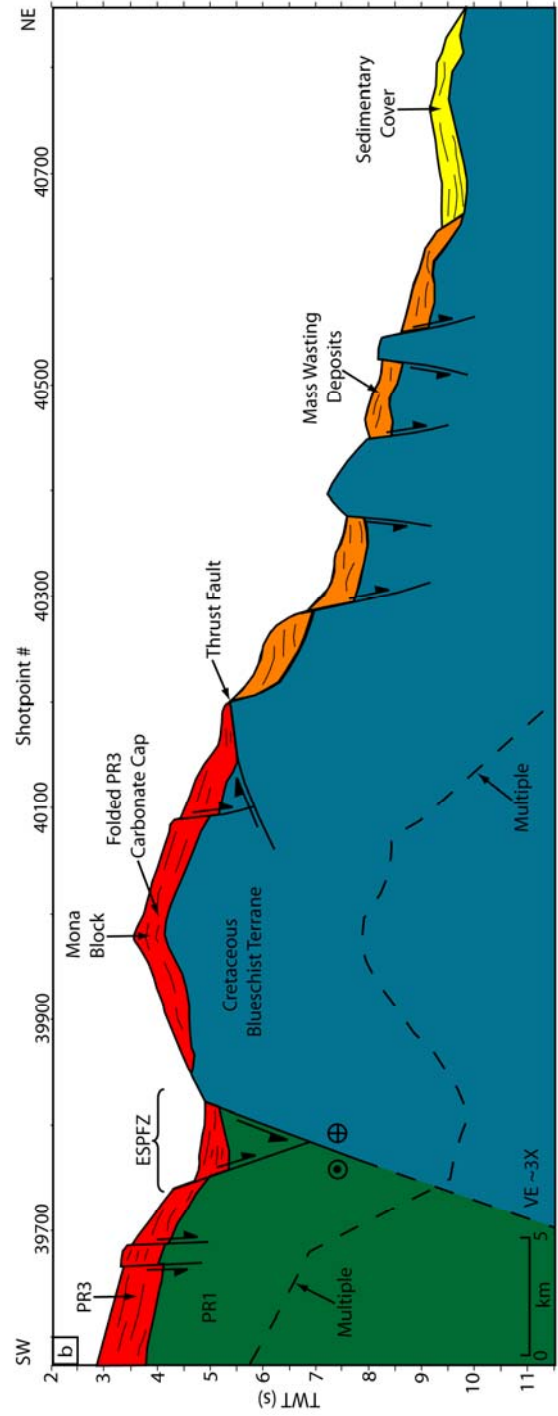
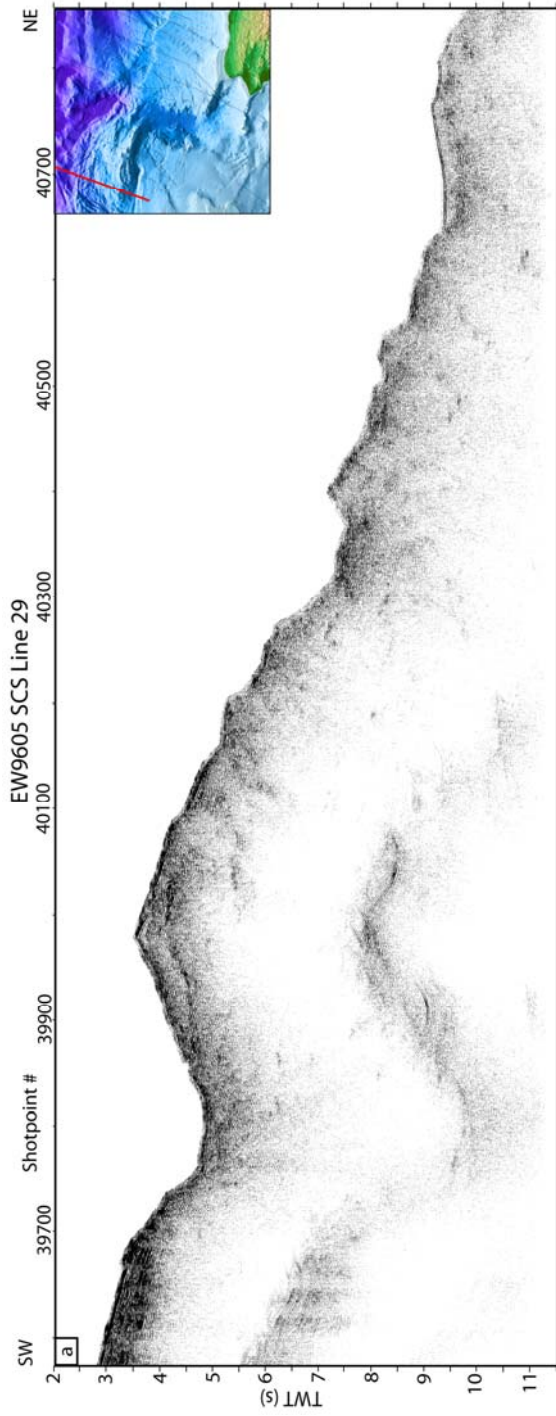


Fig. 17. EW9605 SCS Line 29. West side of Mona Block see index map at top right for exact location of section. a. Processed data. b. Line drawing interpretation of processed data. Dashed line is multiple seafloor reflection. Vertical exaggeration is approximately 3X. Green unit represents PR1, red unit represents PR3, blue unit represents blueschist terrane, orange unit represents mass wasting deposits, yellow unit represents clastic fill.



blueschist facies rocks. Sinistral transpressional displacement along the southeast-trending ESPFZ has folded the PR1 and PR3 rocks, creating a 10 km-wide positive flower structure in a deep valley on the south side of the Mona Block (maximum water depths of over 3 km) (Fig. 15). To the southwest of the ESPFZ, northwest-trending normal faults displace blocks of the carbonate platform and other eroded material towards the ESPFZ lineament. Potential evidence for thrust faults also exist in the volcanic basement and uplifted metamorphic rocks in seismic lines 1291, 27, and 29 (Figs. 15, 16, and 17).

STRUCTURAL RESTORATION OF CENTRAL MONA CANYON

The results and interpretation of the marine geophysical data presented in this study leads to a viable extensional model for the formation of the Mona Canyon. With that in mind, a structural restoration of the central Mona Canyon was attempted to piece together its tectonic evolution. Balanced structural restorations are used to restore geologic cross-sections to their pre-deformational state by reversing brittle and/or ductile deformation (Hossack, 1979; Groshong, 1989; Wu et al., 2005). Balanced structural restorations are also widely used to help validate geophysical interpretations of seismic reflection sections (Gibbs, 1983; Wu et al., 2005). In order to produce a balanced structural restoration, one must assume plane strain, which conserves cross-sectional area in 2-D, or volume in 3-D (Hossack, 1979; Gibbs, 1983; Wu et al. 2005). Although Gibbs (1983) noted that the change in bed area and volume can be greater than 40% due to the effects of compaction, diagenesis, and strain, this assumption is still considered to be reasonable for most restoration applications.

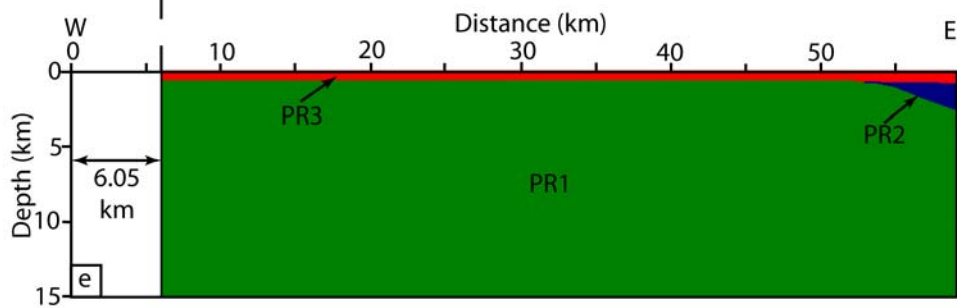
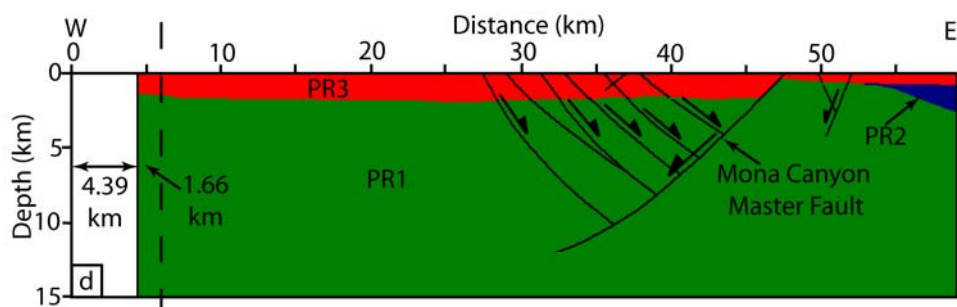
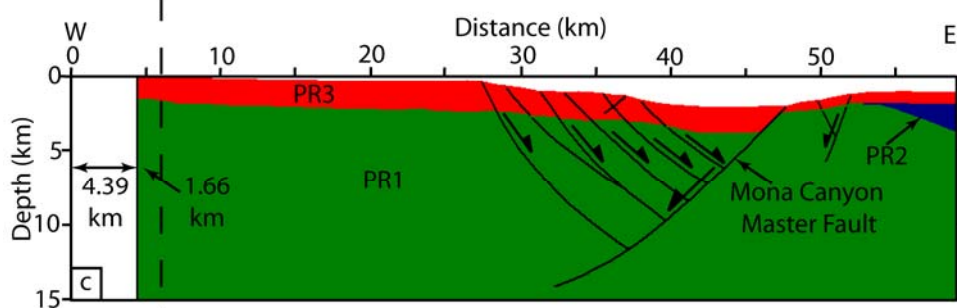
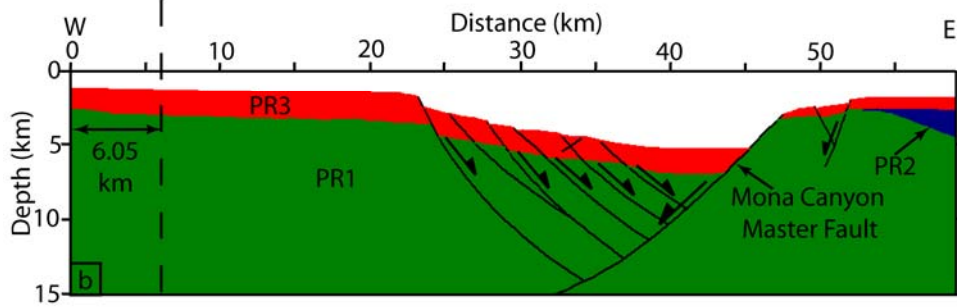
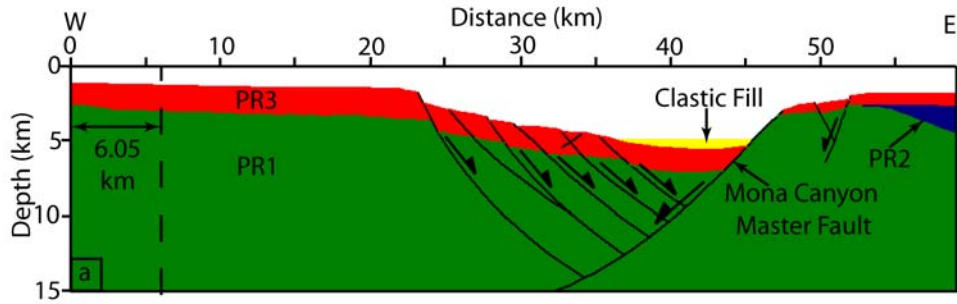
Midland Valley's 2DMove v5.0 software program was used to depth convert and generate a balanced structural cross-section restoration of the interpretation of EW9501 MCS Line 1289 (Fig. 11). This line was chosen for its high resolution, deep penetration, and its approximately perpendicular orientation to the central Mona Canyon, and assumed E-W direction of tectonic extension. However, because EW9501 MCS Line 1289 is slightly oblique to the principal plane of extension, the calculated extension and longitudinal strain will be slightly smaller than the actual value because the study is not restoring the true width of the half-graben (Gibbs, 1983).

As recommended by Gibbs (1983), the section was converted from two-way travel time to depth and maintained at a 1:1 ratio before restoring the section. The depth conversion was performed using interval velocities determined from the velocity analysis of MCS CMP data (Fig. 18a). The water column was assumed to have an interval velocity of 1500 m/s, as is applied to most areas. The clastic fill along the axis of the canyon were calculated to have an interval velocity of 1850 m/s, comparable to seismic velocities of turbidites offshore the Baja Peninsula (Moore et al., 1982). The PRVI carbonate platform, PR3, was calculated to have an interval velocity of 2850 m/s, which is comparable to the velocities for this unit from Western Geophysical (1974), 2700 m/s, Anderson (1991), 2930 m/s, and van Gestel et al. (1999), 2750 m/s. The forearc basin unit, PR2, was calculated to have an interval velocity of 3200 m/s. The volcanic and volcanoclastic basement rocks, PR1, were calculated to have an interval velocity of 5500 m/s, which is close to the 5800 m/s velocity Officer et al. (1959) determined during a seismic refraction study over the Greater Antilles (Officer et al., 1959; Fox and Heezen, 1975; Boynton et al., 1979).

After converting the section to depth, 2DMove was used to generate a reconstructed and balanced cross-section using the inclined shear restoration method to determine the amount of extension, and the approximate timing of events that led to the formation of the central Mona Canyon. This will ultimately help this study propose an approximate age for the half-graben. The inclined shear method described by Xiao and Suppe (1992), Wu et al. (2005) and Fossen et al. (2003) restores hanging wall and footwall cut-offs by moving individual fault blocks back up the fault planes to their approximate pre-displacement locations. Clay models by Xiao and Suppe (1992) and

Fig. 18. Structural restoration of interpretation of EW9501 MCS Line 1289 over central Mona Canyon. Restoration performed using Midland Valley's 2DMove v5.0 software.

a. Seismic section converted to depth and interpreted at 1:1 ratio. Interval velocities derived from velocity analysis of MCS CMP data were utilized for the depth conversion: water column: 1500 m/s; turbidite deposits (yellow unit): 1850 m/s; PR3 (red unit): 2850 m/s; PR2 (purple unit): 3200 m/s; PR1 (green unit): 5500 m/s. b. Turbidites backstripped and effects of strain in PR3 accounted for with isostatic adjustment. c. Hanging-wall and footwall cut-offs at top horizon of PR3 restored using 60° of antithetic shear. d. Top of PR3 flattened to Present day sea level using line-length unfolding. e. Remaining fault displacements in PR1 restored using 60° of antithetic shear, and then top of PR1 flattened to horizontal using line-length unfolding. The restoration yields a minimum extension through the Recent of 6.05 km and a minimum longitudinal strain of 11.4% in the central Mona Canyon.



computational models by Fossen et al. (2003) determined that forward models of half-graben deformation achieved the most geologically reasonable hanging wall geometry when using 60° of antithetic movement along the faults, as opposed to the fault blocks simply dropping down vertically to fill a void created by dip separation on the master fault. Therefore, 60° of antithetic shear was used to reconnect the hanging wall and footwall cut-offs interpreted in EW9501 MCS Line 1289 (Figs. 11 and 18) (Wu et al., 2005).

The forward models described above also suggest that changing the dip of the master fault changes the hanging wall geometry, whereby a steeper master fault creates a steeper hanging wall dip (Xiao and Suppe, 1992; Fossen et al., 2003; Wu et al., 2005). Therefore, the major control on the reconstruction is the dip of the Mona Canyon master fault, which is interpreted to have a listric geometry that has a decrease in dip with depth (Figs. 11 and 18). Groshong (1989) recognized this type of master fault as a subset of the ideal single-bend master fault, where the master fault is composed of two straight-line segments with a single bend that causes a change in dip in the hanging wall. However, the dip of the Mona Canyon master fault interpreted in EW9501 MCS Line 1289 closely matches with analogue solutions that relate the upper and lower master fault dip with hanging wall dip (Groshong, 1989). The upper segment of the Mona Canyon master fault has a seismically-inferred dip of 45° , and combined with the inferred hanging wall dip of 9.5° on the west side of the Mona Canyon, the lower segment of the Mona Canyon master fault should, according to the analogue models, approach a dip of 25° (Groshong, 1989). This is the lower dip of the fault interpreted in Figs. 11 and 18. At depth, this fault may continue to shallow into a flat detachment, or be transitional into a zone of

ductile stretching as it approaches the base of the Greater Antilles island arc crust, which could be as deep as 30 km (Talwani et al., 1959; Groshong, 1989; Larue and Ryan, 1989).

This study also assumes that as displacement along the Mona Canyon master fault increased with time, the antithetic faults on the hanging wall of the half-graben developed from east to west. Therefore, the section was restored from west to east across the half-graben. Because this study restores a single 2-D seismic line, and to minimize speculation about the oblique-slip nature of the Mona Canyon master fault, this study also assumes purely dip-slip motion with respect to plane strain along all faults. Although there is certainly the possibility for oblique-slip motion along the Mona Canyon master fault, assuming strictly normal displacement allows the simplest restoration workflow, and provides the simplest solution for this study.

The clastic fill along the axis of the graben, the yellow unit, was first backstripped using default values for porosity (56%) and the amount which the porosity decreases with depth due to compaction ($0.39 \times 10^{-5} \text{ cm}^{-1}$) (Fig. 18b); (Sclater and Christie, 1980). This decompaction is based on the exponential compaction/decompaction function of Sclater and Christie (1980), and also applies an isostatic adjustment in the underlying layers due to the removal of this unit.

After removing the clastic fill, the hanging wall and footwall cutoffs of the individual fault blocks were restored to their approximate predeformation condition using the 60° antithetic shear restoration method (Fig. 18c). Because this restoration method does not remove rollover folding in the hanging wall blocks, an additional line-length unfolding algorithm was used to flatten the top of the PRVI carbonate platform, the red

unit, to Present day sea level (Fig. 18d). The line-length unfolding algorithm restores a template line, the PR3 horizon, to a user-specified datum, here being present day sea level. Any horizons below the template lines are moved passively (Wu et al., 2005). This method does not maintain line length; only the area between the beds is maintained. However, the change in line length is minimal for shallow-dipping beds such as those interpreted in the hanging wall of the central Mona Canyon.

After restoring PR3 to present day sea level, the remaining vertical and horizontal components of dip separation in the footwall and hanging wall cutoffs in the basement rocks, the green unit, were restored using the 60° antithetic shear restoration method (Fig. 18e). Any rollover folding remaining in the basement horizon was then removed using the line-length unfolding algorithm (Fig. 18e).

Two separate phases of minimum extension are observed in the 60° antithetic shear structural restoration results (Fig. 18). This restoration method yields an initial minimum 1.66 km of extension, followed by a second, later phase of 4.39 km for a minimum extension of 6.05 km through the Recent (Fig. 18). Because the initial length of EW9501 MCS Line 1289 is 59.062 km, the restoration suggests a minimum longitudinal strain of 11.4% across the central Mona Canyon.

DISCUSSION

Based on the interpretations of the marine geophysical data, this study can now evaluate the compatibility of the three tectonic models described in the Introduction with the Mona Canyon. The supporting and/or non-supporting evidence for each model as they apply to the Mona Canyon is described below.

Comparison of Evidence with Proposed Tectonic Models

Pinning and Extension Model

Several pieces of evidence in the Mona Canyon appear to be compatible with the pinning and extension model. The main piece of evidence in support of this model is the extensional faults interpreted throughout the study area. The differential GPS velocities between Hispaniola and the PRVI microplate provide additional supporting evidence for the pinning and extension model (Fig. 1); (Calais et al., 2002; Mann et al., 2002).

Displacement vectors indicate that Puerto Rico and the Virgin Islands are moving to the northeast faster than Hispaniola relative to a fixed North American plate. Slip-analysis studies of onshore faults mapped in Neogene carbonates around Aguadilla by Hippolyte et al. (2005) also supports the proposed E-W direction of opening in the Mona Canyon indicated in the pinning and extension model (Fig. 10).

The pinning and extension model indicates that the E-W direction of extension and differential movement of Hispaniola and Puerto Rico-Virgin Islands microplate would produce a generally north-trending half-graben. This configuration is compatible with the current interpretation of the central Mona Canyon. Additional potential evidence for the pinning and extension model includes thrust faults interpreted in the

seismic sections in the region of the Mona Block, which may have been caused by the oblique subduction of the Bahamas Platform (Figs. 15, 16, 17, 19, and 20). Fig. 19 depicts an observable cluster of shallow crustal earthquakes, depths less than 20 km, that appear to outline the northwest-southeast-trending lineament of the Bahamas platform. Shallow, <20 km depth, focal mechanisms indicate apparent thrust motion on the east and west side of the Mona Canyon, which may be caused by the oblique subduction of the NOAM plate and the collision with the Bahamas Platform (Fig. 19). The single focal mechanism in the central Mona Canyon indicates normal motion (Fig. 19).

However, the pinning and extension model does not readily explain the orientation of the northwest-trending southern and northern domains of the Mona Canyon. This model implies the Mona Canyon should be a generally north-trending graben. However, sinistral transpression due to the oblique collision of the North American and Caribbean plates may cause rigid body rotation between these two domains (Fig. 2). Therefore, there may be an E-W extensional component that is opening the Mona Canyon, and a sinistral transpressional component that is simultaneously rotating the southern and northern domains of the Mona Canyon. This would indicate strain partitioning between the southern, central, and northern domains of the Mona Canyon, which may be being accommodated by the GSPRFZ near the southern domain, and the East Septentrional and Bowin fault zones between the central and northern domains (Fig. 19). However, the implied sinistral motion suggested by orogen-parallel extension should act to close the southern and central regions of the Mona Canyon because this region would be a domain of shortening in a transpressional plate boundary.

Fig. 19. Earthquake-fault map over Mona Canyon. Illumination is from the south. Black lines are faults interpreted from seismic reflection data, multibeam bathymetry, and sidescan sonar data; solid were exposed, dashed where concealed. Yellow filled circles are earthquakes of magnitude 3.0 and greater and depths less than 20 km from USGS NEIC online earthquake database from 1973 to 2007, includes PRSN data. Black focal mechanisms are from the Harvard Centroid Moment Tensor online database from 1976-2007 and Doser et al., 2005, depths less than 20 km; labeling includes date and depth. The red focal mechanism is for the M7.2 1918 event from Doser et al., 2005, and is geographically accurate to within 50 km. The depth of this event ranges from 20 +/- 7 km. The size of the focal mechanism solution is relative to the magnitude of the earthquake. The dashed red line defines the 90% confidence ellipse for location of the 1918 earthquake after Doser et al. (2005). The dashed white line defines the 18 km isobath for the interface of the subducting North American slab after Laforge and McCann (2005). The dashed magenta line outlines an observable earthquake cluster that may be caused by the oblique subduction of the southeast end of the Bahamas platform and subsequent uplift of the Mona Block. ESPFZ – East Septentrional Fault Zone, GSPRFZ – Great Southern Puerto Rico Fault Zone.

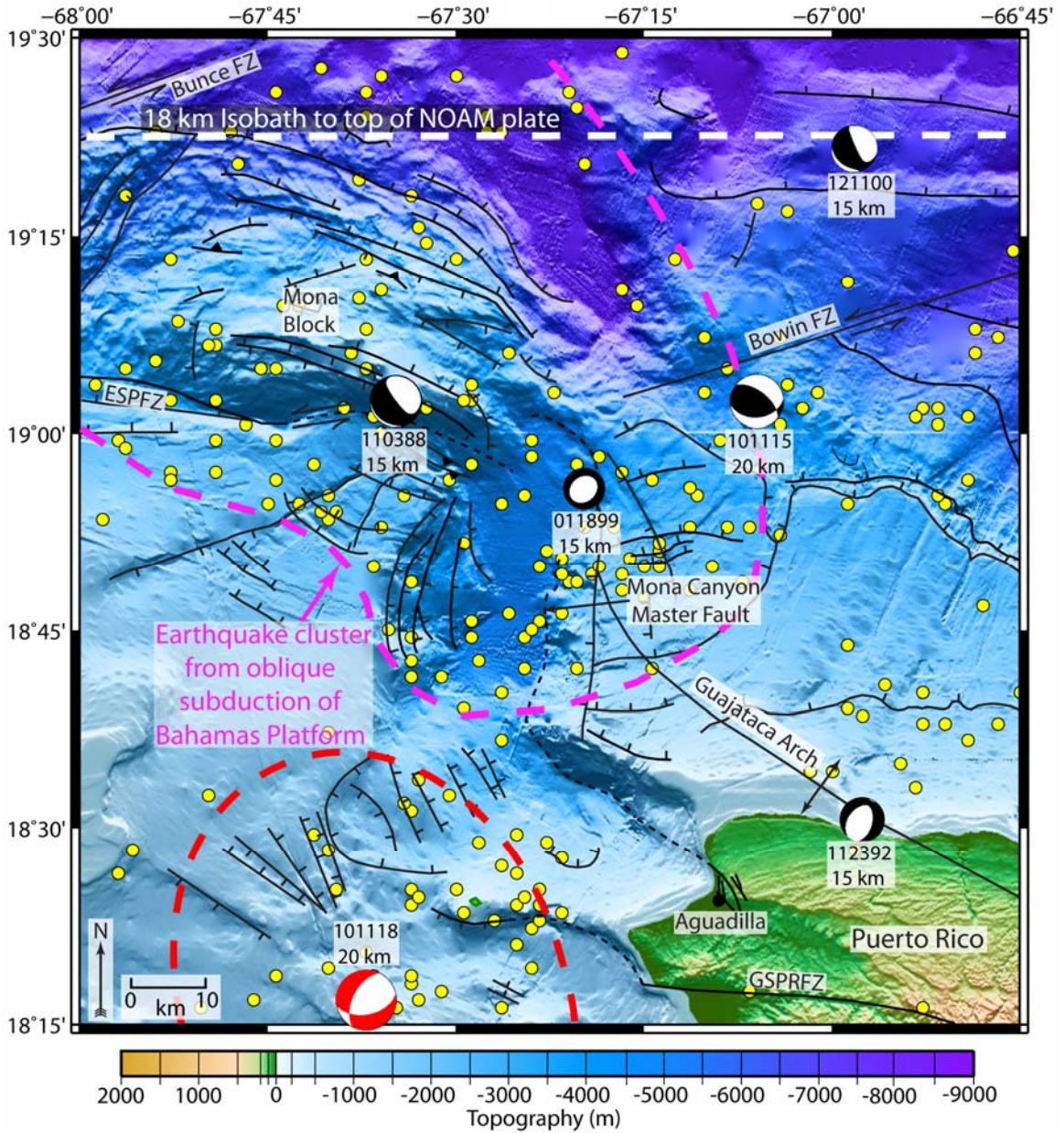
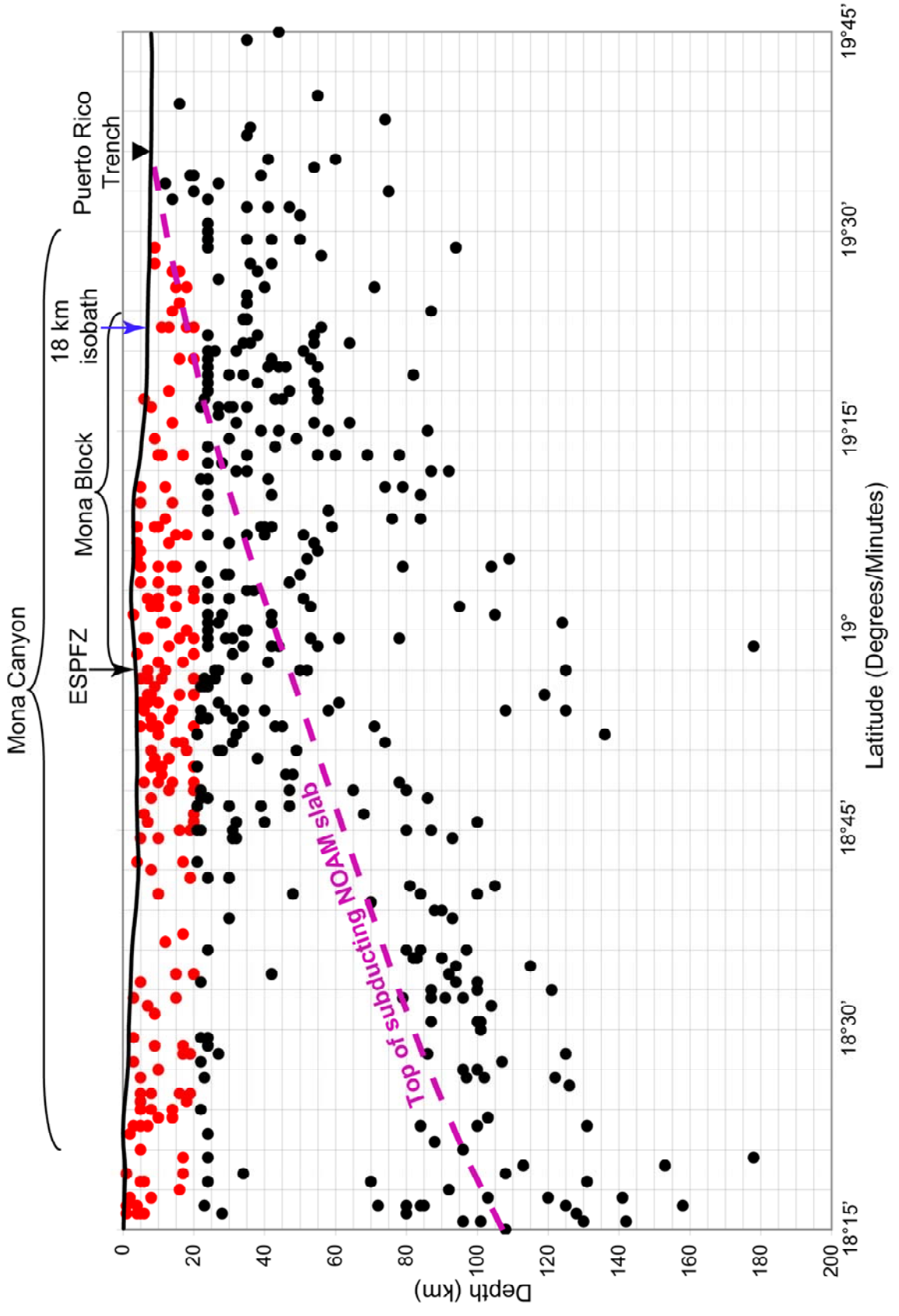


Fig. 20. Vertical earthquake profile across the Puerto Rico trench and the Greater Antilles island arc from -67°W to -68°W longitude, $18^{\circ}15'\text{N}$ to $19^{\circ}30'\text{N}$ latitude. Black line is the seafloor profile across $-67^{\circ}30'\text{W}$. 1973-2007 earthquakes are from the USGS NEIC database, including PRSN data. Red dots are earthquakes plotted in Fig. 19 over the Mona Canyon study area; M3.0 and greater, depths less than 20 km. Black dots are earthquakes outside of region shown in Fig. 19, M3.0 and greater, maximum depth of 200 km. Earthquakes assigned default depths of 25 and 33 km are not included. Dashed magenta line is the top of the subducting North American (NOAM) slab. Blue arrow denotes trace of 18 km isobath shown in Fig. 19. Black arrow denotes trace of ESPFZ shown in Fig. 19.



Rotating Block Model

Paleomagnetic data from the PRVI carbonate platform, PR3, indicates $24^{\circ} \pm 5.8^{\circ}$ counterclockwise rotation of Puerto Rico from approximately 11-4.5 Ma (Reid et al., 1991). This approximately 24° rotation may have caused the extension in the Mona Canyon (Masson and Scanlon, 1991). The proposed rotation and arc-normal extension of Masson and Scanlon (1991) and Reid et al. (1991) appears to correlate with the rotating block model of Geist et al. (1988) and Dobson et al. (1996). However, there are four problems with using the rotating block model to explain the formation of the Mona Canyon. The rotating block model indicates the Mona Canyon would result from dextral strike-slip and normal faults that bound the walls of the canyon (Fig. 3) (Geist et al., 1988). Seismic reflection data can only resolve the vertical component of displacement. Though dextral and sinistral faults may be present in the study area, they cannot be resolved in the seismic data. The rotating block model also suggests a dextral tear-fault along the south side of the Mona Block should control a summit basin in the area of the hanging wall of the Mona Canyon. Although the thicker section of carbonate strata indicates this area is a basin, the one focal mechanism solution in the central Mona Canyon suggests primarily normal displacement and the relative GPS velocities also suggest sinistral motion (Figs. 1 and 19); (Calais et al., 2002; Mann et al., 2002). There should also be evidence for similar summit basins and transverse canyons across the Greater Antilles island arc that would bind multiple rotating blocks as indicated by the model in Fig. 3. However, this is the only proposed tectonically-controlled submarine canyon in the Greater Antilles.

However, the rotating block model would produce the northwest-trend of the southern and northern Mona Canyon domains. It may be possible that this rotation was initiated through the counterclockwise rigid block rotation of Puerto Rico, increasing the rate of rifting and creating the en-echelon shape of the Mona Canyon (Masson and Scanlon, 1991; Reid et al., 1991).

Incised Canyon Model

Several pieces of evidence exist in the Mona Canyon that are compatible with the incised canyon model shown in Fig. 4. The most obvious of these is the Mona Block, where this study interprets thrust faults in the seismic reflection data, as well as the shallow crustal earthquakes that appear to form a cluster in the same orientation as the northwest-southeast-trending Bahamas Platform lineament (Figs. 15, 16, 17, and 19). Possible evidence for post-Pliocene NE-SW-directed shortening from underthrusting is also interpreted in EW9605 SCS Line 25, which shows potentially folded sedimentary sequences in the central Mona Canyon on the southern side of the Mona Ridge (Figs. 10 and 13). The underthrusting of the SE Bahamas, which began to impact the Mona Canyon region approximately 5 Ma, and the uplift of the Mona Block, may be linked with the folding of the sedimentary sequences in the central Mona Canyon. This study proposes that the Mona Ridge is the eastward extension, i.e. the easterly limb, of the Mona Block. There are also extensive amounts of mass wasting deposits in the northern Mona Canyon, both along the walls and its axis (Figs. 10, 13, 14, and 15). The greater than 1 km-thick mass wasting deposits in the northern domain provide additional evidence for the headward erosion indicated in the description of this model (Fig. 4).

However, there are five main problems with using the incised canyon model to describe the formation of the Mona Canyon. The most important piece of potential evidence that contrasts the incised canyon model is the extensional faults interpreted in the marine geophysical data. Also, if the canyon had formed from headward erosion as the forearc was uplift, then the northern region should be oriented to the northeast because the Bahamas has swept across the margin from northeast to southwest (Fig 4). Interpretations of the marine geophysical data in this study indicate the northern Mona Canyon is oriented northwest-southeast, which is opposite to the expected orientation. Therefore, the trend of the northern Mona Canyon and the trend of the subduction of the Bahamas platform do not match. There is also no observable evidence for the landward transition of the Mona Canyon into a narrow furrow as hypothesized in the incised canyon model (Fig. 4); (Laursen and Normark, 2002). As interpreted in this study, the canyon maintains an average 25 km-width along its entire length. This model also has the problem that typical erosional processes do not usually form such a large submarine canyon. Canyons traditionally identified as having been carved by rivers during sea level low stands and/or turbidity currents have steeper, across-axis v-shapes, and maximum widths less than 10 km. This includes the Monterey submarine canyon off the coast of California, as well as submarine canyons of the coast of Massachusetts, the north coast of Hawaii, and the margins of Alaska, France, Congo, and Japan (Shepard, 1981). The Bahamas platform is also hypothesized not to have subducted further south of the Mona Ridge, so it could not have been able to form the central and southern domains of the Mona Canyon. Therefore, the incised canyon model has likely played a role in the formation of the northern Mona Canyon through headward erosion and mass wasting

processes, but because the deformation from the subduction of the Bahamas platform as indicated by the cluster of shallow crustal earthquakes in Fig. 19 has not progressed south of 18°36'N, it likely did not cause the morphology and structure seen in the southern and central regions.

Summary of Tectonic Models

Based on the evidence for extensional faulting in the marine geophysical data, the differential movement of Hispaniola relative to the PRVI microplate, the focal mechanism solutions on the east and west sides of the Mona Canyon, and the interpreted cluster of shallow crustal earthquakes in the region of the Mona Block, the pinning and extension model after Mann et al. (2002) provides the most compatible interpretation for the formation of the Mona Canyon, and is the model advocated here. The Rotating Block model of Geist et al. (1988) and Dobson et al. (1996), and the Incised Canyon model of Laursen and Normark (2002), have likely played minor roles in the formation of the northern Mona Canyon through counter-clockwise rotation and headward erosion, respectively, but are insufficient in accounting for all the evidence presented in the southern and central regions. This conclusion is based on the lack of summit basins, other transverse canyons, and the presence of extensional faults in the Mona Canyon.

Tectonic Evolution of Central Mona Canyon

Based on the results presented in this study, an extensional model for the formation of the Mona Canyon appears to work best. If the structural restoration presented here is viewed in reverse, i.e. in the forward modeling perspective (Fig. 18e through 18a), the evolution of the formation of the central Mona Canyon half-graben can

be proposed. The results of the structural restoration suggests that the central Mona Canyon is older than the previous estimate of 1.2 million years old that was calculated using the 5 mm/year GPS rate of extension in the northern Mona Passage (Mann et al., 2002). The structural restoration suggests that the central Mona Canyon may have experienced two phases of development described in detail below. Major tectonic changes along the northern Caribbean plate boundary are proposed to have initiated these two phases.

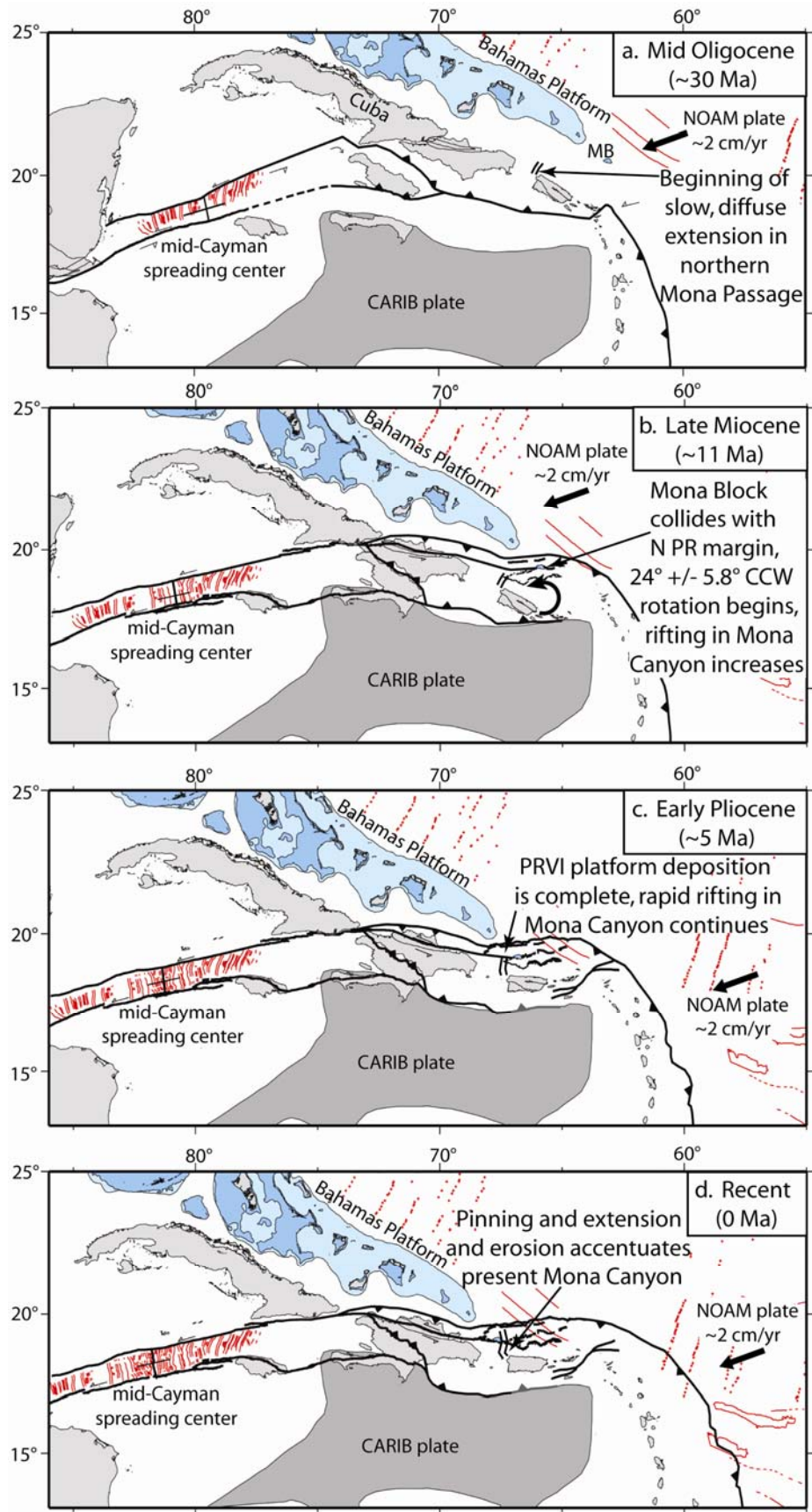
These two phases of development of the central Mona Canyon illustrated in the structural restoration are used in this study to account for the evolution of the entire Mona Canyon. However, it is possible that the southern, central, and northern Mona Canyon domains are not all the same age, which is of particular concern in the northern Mona Canyon where the stratigraphic control on the shallow water PRVI carbonate platform, PR3, does not exist. The lack of the PR3 stratigraphic control in the northern Mona Canyon makes it difficult to determine if the entire canyon formed simultaneously, or if different processes and tectonic regimes formed the three domains at different times. Unfortunately, there is not enough data, specifically well data, to constrain this issue, or to distinguish the possible differences in evolution between the southern, central, and northern domains of the Mona Canyon. Therefore, the following discussion develops a hypothesis that the evolution of the central Mona Canyon shown in the structural restoration is representative of the formation of the entire bathymetric feature.

This study proposes the following two-phase tectonic evolution for the Mona Canyon as illustrated in Figs.18 and 21:

Tectonic Phase I: Initial Rifting in Central Mona Canyon: Middle Oligocene to Late Miocene

Figs. 18e and 21a depict major tectonic activity in the central Mona Canyon through the Middle Oligocene, approximately 30 Ma. Through this stage, the Late Cretaceous to Middle Eocene Greater Antilles island arc massif, PR1, has formed. The deposition of a distal fan of the Late Eocene volcanoclastic forearc wedge, PR2, precedes the island arc massif formation, and then the Middle Oligocene to Late Miocene/Early Pliocene PRVI carbonate platform, PR3, begins to be deposited. In the Middle Oligocene through the Late Miocene, approximately 30-11 Ma, an initial, early stage of extension of 1.66 km occurs in the Mona Canyon (Figs. 18d and 21b). Back-tilting and uplift of the footwall block on the east side of the Mona Canyon, and vertical and westward-directed displacement of the hanging wall block on the west side of the canyon may have accompanied this initial extension, as is noted in typical half-graben settings (Groshong, 1989). This slow, possibly diffuse, 0.087 mm/year extension created extra accommodation space necessary to deposit a thicker section of PR3 on the hanging wall. Extension created extra space for deposition of the platform on the hanging wall, yet was slow enough not to drop the hanging wall below 100-200 m water depth where the depositional sequence would be shut down because the reefs needed light to grow. Because the footwall is proposed to be likely higher during this time, it allowed only a minimal amount of the carbonate material to be deposited on the east side of the Mona Canyon. In this proposed scenario, the hanging wall also must collapse relatively vertically so that an asymmetric wedge in the form of growth strata of PR3 does not form in the axis of the Mona canyon (Xiao and Suppe, 1992). This would explain the lack of

Fig. 21. Plate tectonic reconstructions of the northeast Caribbean Puerto Rico trench – SE Bahamas collision zone for four intervals. Reconstruction is modified after Mann et al. (2002), and is based on paleomagnetic lineations on the North American (NOAM) and Caribbean (CARIB) plates. These lineations are the red lines indicated on the NOAM plate, and in the Cayman trough. Motion is relative to a fixed Caribbean plate, and Cuba and the Bahamas carbonate platform (dark blue represents high-standing banks, light blue represents deeper banks) are moved with the subducting North American plate. Gray shaded region is a large igneous province on the Caribbean plate. a. Note the Mona Canyon is created in the Middle Oligocene, approximately 30 Ma. b. In the Late Miocene, approximately 11 Ma, the southeast corner of the Bahamas carbonate platform known as the Mona Block (MB) collides with the northern Puerto Rico margin. This collision initiates the $24^{\circ} \pm 5.8^{\circ}$ counterclockwise rotation of Puerto Rico, and may have increased rifting in the Mona Canyon. c. When the Bahamas platform reaches its current position in the Early Pliocene, approximately 5 Ma, and the youngest unit of the PRVI carbonate platform, PR3, deposition is completed, rifting in the Mona Canyon continues to increase more rapidly through the Recent (d). Erosion via submarine mass wasting transport towards the Puerto Rico trench accompanied pinning and extension between Hispaniola and Puerto Rico, subsequently accentuating the morphology of the northern Mona Canyon.



asymmetry of PR3 near the axis of the canyon (Figs. 11 and 18). The sub-vertical hanging wall collapse may have been facilitated by a steeper, possibly sub-vertical, Mona Canyon master fault during this time, which then became shallower and listric through the Recent.

Two major events, individually or combined, may be responsible for this initial rifting in the northern Mona Passage that began in the Middle Oligocene approximately 30 Ma. The first event of interest is sinistral strike-slip displacement along the GSPRFZ in the Paleocene to Early Oligocene. This event is correlated with Eocene rifting and infilling of a northwest-trending basin south of the GSPRFZ in central Puerto Rico (Erikson and Pindell, 1991). The second event of interest is the initiation of seafloor spreading in the Cayman trough in the Early Eocene to Late Oligocene (Macdonald and Holcombe, 1978; Wadge and Burke, 1983; Rosencratz et al., 1988; Edgar et al., 1989; Ladd et al., 1990). The mid-Cayman spreading center formed between 50 and 25 Ma, and experienced at least 284 km of spreading since the Late Miocene, yielding an average spreading rate between 1.5 and 4 cm/year (Macdonald and Holcombe, 1978; Pindell and Barrett, 1990). Although the rate of seafloor spreading in the mid-Cayman trough is significantly higher than that determined in the Mona Canyon at 1.5-4 cm/year and 0.087 mm/year, respectively, it is possible that far-field extensional stress was transferred along the sinistral Septentrional fault zone, may have acted as a transform fault during this time, into the Mona Passage to enhance rifting in the Mona Canyon.

These regional events are proposed to be responsible for the slow, initial rifting in the Mona Canyon because the Middle Oligocene to the Late Miocene, approximately 30-11 Ma, was likely a tectonically quiet period along the northern Puerto Rico margin to

deposit the shallow water PRVI carbonate strata, PR3 (Monroe, 1980; Larue, 1991; van Gestel et al., 1999). Also, to deposit a complete section of this shallow water carbonate strata at the base of the Mona Canyon at over 5 km water depth, but still be able to deposit a sequence that is nearly twice as thick as shown in Figs. 11 and 12, rifting most likely had to begin very slowly and continue throughout the deposition of PR3 from the Middle Oligocene to at least the Late Miocene, or else the reefs would not have had light to grow. These regional events would also account for the seemingly slow initial rate of rifting, which was required to create the additional accommodation space necessary for the thicker sequence of carbonate strata on the hanging wall.

The proposed age of the Mona Canyon suggests that this area was a deepwater impediment for biota migrations starting in the Middle Oligocene. Paleogeography studies of Iturralde-Vinent and MacPhee (1999) and MacPhee et al. (2003) propose the Mona Passage was a shallow water area or landbridge through the Middle Miocene, approximately 16-11 Ma. However, MacPhee et al. (2003) note that the rifting in the Mona Canyon could not have been initiated any earlier than Middle Oligocene, approximately 30 Ma, because of paleontological evidence of land mammals correlated between Hispaniola and Puerto Rico until this time. This paleontological evidence limits the possibility for a date earlier than the Middle Oligocene for the initiation of rifting in the Mona Canyon, and also limits the possibility for an asymmetric wedge of the Late Eocene PR2 forearc basin in the half-graben, which helps to back-up the interpretation of the seismic reflection data and the structural restoration of the central Mona Canyon presented in this study.

Tectonic Phase II: Later Rifting in Central Mona Canyon: Late Miocene to Recent

In the Late Miocene to Early Pliocene, approximately 11-5 Ma, the deposition of the PRVI carbonate platform, PR3, is completed (Figs. 18c and 21b and 21c); (Larue, 1991; van Gestel et al., 1998; van Gestel et al., 1999). The structural restoration presented in this study suggests that the completion of the deposition of PR3 is accompanied by a rapid increase in rifting from 0.087 to 0.4 mm/year, causing an additional minimum extension of 4.39 km. This sudden increase in extension resulted in hanging wall collapse and rapid subsidence (Figs. 18c and 18b). Thus, from the Late Miocene through the Recent, there has been a minimum extension of 6.05 km in the central Mona Canyon. Antithetic faults bounding several rider blocks are proposed to have developed from east to west, eventually leading to the current antithetic faults in the hanging wall (Fig. 18b). Continued erosion of the fault blocks accompanied this extension, forming syndepositional clastic basin-fill deposits in the canyon axis (Figs. 18a and 18b and 21c and 21d).

The rapid, late-stage extension of 4.39 km, as compared to the slow, initial stage of 1.66 km, has presumably played the most important tectonic role in the formation of the Mona Canyon because it likely caused the majority of the hanging wall collapse as proposed in the structural restoration (Fig. 18). Two major tectonic events that occurred at the same time along the northern Caribbean plate boundary zone may have caused the proposed rapid post-Late Miocene rifting in the Mona Canyon. The first is the collision between the Bahamas platform and the northern margin of Puerto Rico in the Late Miocene to Late Pliocene, approximately 11-3 Ma (McCann and Sykes, 1984; Dolan et

al., 1998; Dolan and Wald, 1998; Mann et al., 2002; McCann, 2002; Grindlay et al., 2005; Mann, 2005). And $24^{\circ} \pm 5.8^{\circ}$ counterclockwise rotation of Puerto Rico in the Late Miocene to Early Pliocene, approximately 11-4.5 Ma, as determined from paleomagnetic data in the PRVI carbonate platform, PR3 (Masson and Scanlon, 1991; Reid et al., 1991).

It is proposed here that the collision of the Bahamas platform with the northern margin of Puerto Rico initiated the $24^{\circ} \pm 5.8^{\circ}$ counterclockwise rotation (Fig. 21b). As the Bahamas platform approached slightly east-northeast of its present position 11 Ma, the Mona Canyon may have served as a pre-existing weakness in the Greater Antilles crust from the previous phase of extension, and failed readily. The northeast to southwest collision of the Bahamas platform with the northern Puerto Rico margin may have simultaneously initiated the counterclockwise rotation of the Puerto Rico block, and increased the rate of rifting in the northern Mona Passage (Masson and Scanlon, 1991).

The combination of counterclockwise rigid body rotation of the Puerto Rico block and pinning and extension from the collision of the Bahamas platform with Hispaniola and the northern Puerto Rico margin is proposed to have accelerated the rate of extension in the Mona Canyon to 0.4 mm/year beginning approximately 11 Ma (Figs. 18 and 21). This second phase of accelerated extension possibly led to hanging wall collapse and full development of the half-graben through the Recent. Erosion of the fault blocks accompanied this extension, depositing clastic basin-fill sediments into the axis of the canyon. Mass wasting material was also likely transported north towards the Puerto Rico trench from the bathymetrically higher areas in the southern and central Mona Canyon, and from the proposed uplift referred to as the Mona Block, helping to erode the deeper,

northern domain of the Mona Canyon. These processes have likely accentuated the morphology of the northern Mona Canyon domain through the Recent (Fig. 21d).

Tsunami Implications

Tsunamis are abnormally large waves that inundate near shore areas, and are typically generated by shallow, less than 20 km depth, earthquake-induced seafloor faulting or submarine landslides that subsequently displace the water column (Tappin et al., 2000). It is also possible for a combination of fault-related seafloor displacement and submarine mass wasting to generate a tsunami (Tappin et al., 1999, 2000). This combination is particularly linked to producing the 1998 Papua, New Guinea tsunami (Tappin et al., 1999, 2000; Heinrich et al., 2001).

On October 11, 1918 a M7.2 earthquake, initially determined to have originated 40 km off the northwest coast of Puerto Rico, generated a 4-6 m-high tsunami that inundated the northwest coast of the island. The source mechanism of the tsunami is not fully understood. Mercado and McCann (1998) used a data set of low-resolution MCS records to define the seafloor rupture location and displacement along the north-trending Mona Canyon fault in order to numerically model the generation and onshore run-up of the 1918 Puerto Rico tsunami. Mercado and McCann (1998) used 4 m of fault-related seafloor displacement along four segments of the Mona Canyon master fault ranging in length between 4 and 31 km and striking 185-236° to model the run-up of the 4-6 m-high 1918 Puerto Rico tsunami. The bathymetry data used by Mercado and McCann was not dense enough to provide detailed images of potential slump blocks in the Mona Canyon.

The Mercado and McCann (1998) model therefore does not include submarine mass wasting contributions to the 1918 tsunami.

This study has not observed evidence for the southern most segment of the Mona Canyon fault used in the Mercado and McCann (1998) model. The marine geophysical data presented here indicates the Mona Canyon controls the half-graben structure of the southern domain of the Mona Canyon, and is interpolated to connect with the onshore faults mapped around Aguadilla (Figs. 10 and 19); (Hippolyte et al., 2005). Mercado and McCann used a fault dip between 34° - 85° in their model, while this study suggests the Mona Canyon master fault has a dip of 45° and listrically shallows to approximately 25° at depth.

To add complexity to finding a potential source mechanism for the 1918 Puerto Rico tsunami, the uncertainty in locating such an old earthquake could be as great as 50 km geographically, which adds the possibility of this event occurring on the offshore extension of the Great Southern Puerto Rico Fault Zone (GSPRFZ) (Figs. 1 and 19). Doser et al. (2005) have relocated the earthquake used by Mercado and McCann (1998) out of the south-central Mona Canyon, off of the Mona Canyon fault, and into the central Mona Passage using a modern waveform inversion technique, known as the “bootstrap” technique (Fig. 19). Further analysis of the waveform data also suggests that the M7.2 1918 earthquake was a “slow” (i.e. longer seismograph record) earthquake with respect to typical subduction zone earthquakes. Slow earthquakes can sometimes be attributed to slide motion after the initial rupturing (Doser, 2007, personal communication).

The results of the Mercado and McCann (1998) numerical tsunami model depicts a maximum 6 m-high wave arriving at the northwest tip of Puerto Rico 4-6 minutes after

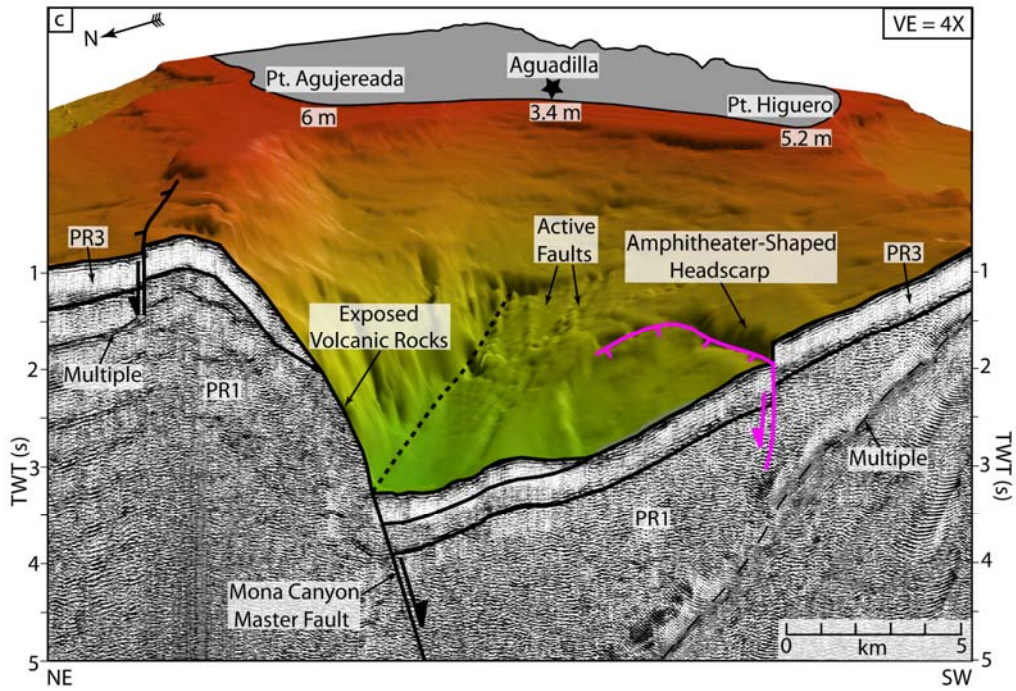
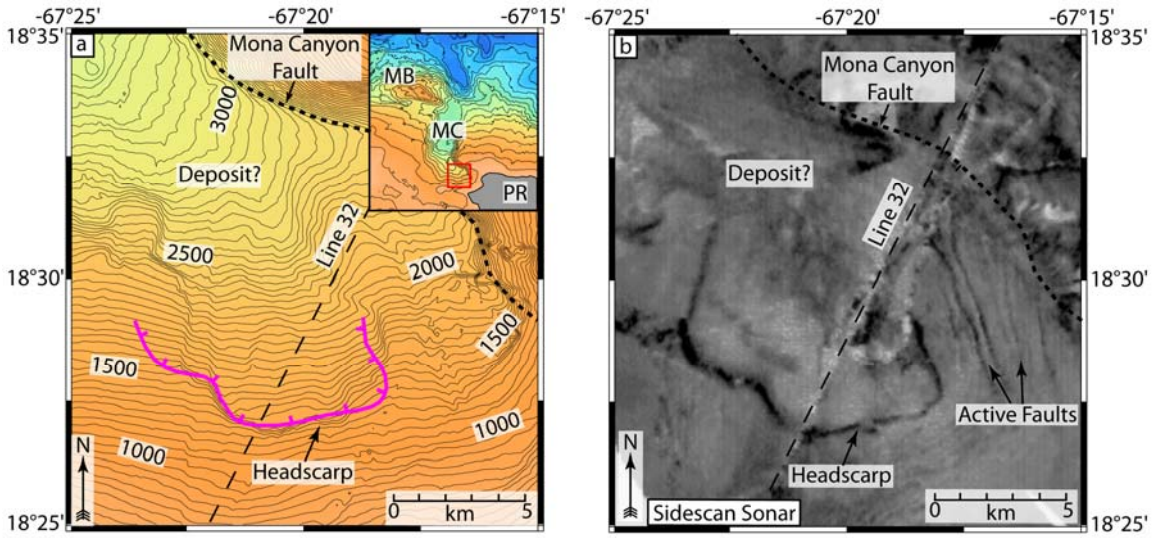
the earthquake, which matches well with observations (Reid and Taber, 1919). Although their results closely match the observed near-field tsunami heights of 4-6 m on the north, west, and northwest coasts of Puerto Rico, there are discrepancies between the model and observations, including the wave amplitude, phase, and timing. These model discrepancies are especially noted in Boquerón Bay, where the modeled wave is 1 m higher than the observed run-up height. Their model also does not take into account wave amplitudes, phase, and timing in far-field areas, including Mona Island in the southern Mona Passage, the east coast of Hispaniola, and the Bahamas (Mercado and McCann, 1998). These wave parameter discrepancies, the “slow” earthquake, the small region of high, greater than 4 m, run-up around Pt. Agujereada, and the rapid attenuation of the wave along the northwest coast of Puerto Rico suggests sediment slumping may have been the source mechanism for the 1918 tsunami (Hornbach et al., 2007).

This study presents evidence for at least 15 active faults having lengths greater than 20 km and minimum displacements of tens of meters throughout the study area, the largest of which appears to be at least 3.5 km of vertical component of dip separation along the Mona Canyon fault (Figs. 10, 11, and 19). These active faults correlate well with the locations of recent shallow earthquakes (Figs. 19 and 20). This is particularly true with the offshore extension of the GSPRFZ, the Mona Canyon fault, the ESPFZ, and the Mona Block. The correlation of the faults with earthquakes, the well-defined lineaments in the bathymetric and sidescan sonar data, and the apparent offsets of surficial seismic reflectors suggest that these structures have likely been active over the past 10,000 years.

Mass wasting deposits, including slumps, slides, flows, and avalanches, are located along the entire length of the Mona Canyon, as well as around the Mona Block in the multibeam bathymetry, sidescan sonar, and in the seismic reflection data (Grindlay et al., 2005; Mondziel, 2007). Of particular interest is a 7 km-wide and 200 m-high amphitheater-shaped headscarp identified at 1.2 km water depth approximately 18 km off the northwest coast of Aguadilla, Puerto Rico, in the southern Mona Canyon (Fig. 22). This headscarp is located in the same region as two submarine cable breaks first noted by Reid and Taber (1919) (Fig. 22). Heezen and Ewing (1952) were among the first to note that sediment slumping can cause submarine cable breaks, including after the 1929 Grand Banks, Newfoundland, earthquake. However, due to the widely spaced seismic sections (e.g. 15 km between EW9605 SCS Lines 32 and 35) the present location of the deposit is unknown. It is possible the displaced material was channeled down and deposited along the axis of the southern Mona Canyon. The data also provide evidence for at least four northwest-trending, 4.5-6.5 km-long faults that break submarine sediments. These faults correspond to active faults first noted during the NR-1 submarine dives by Gardner et al. (1980).

Although the present location of the deposit from the submarine slope failure in the southern Mona Canyon is unknown, the fact that it is located in the same region as the submarine cable breaks is compatible with it occurring during the 1918 event (Fig. 22). This study proposes that the October 11, 1918 M7.2 earthquake re-activated motion along the antithetic fault on the hanging wall of the southern Mona Canyon identified in Figs. 9 and 22. Movement along this fault triggered a slope failure that subsequently broke the submarine cables as it traversed down slope, displaced the water column, and generated

Fig. 22. Southern Mona Canyon mass wasting feature. Magenta line is mass wasting fault contact; dotted line is inferred trace of concealed Mona Canyon fault. a. Bathymetric-contour map of southern Mona Canyon in region of submarine cable breaks caused during the 1918 earthquake and tsunami as noted by Reid and Taber, 1919. Grid interval is 100 m, contour interval is 50 m. Note index map at top right for reference; PR – Puerto Rico, MC – Mona Canyon, MB – Mona Block. b. Sidescan sonar map over same region as (a). Note faults breaking surficial sediments as first described by Gardner et al. (1980). c. Perspective view of southern Mona Canyon showing bathymetry with cut-away showing EW9605 SCS Line 32 (with 500 ms AGC added) over same mass wasting feature. View is from the northwest. Illumination is from the south. Vertical exaggeration is 4X. The numbers on the northwest coast of Puerto Rico are the observed tsunami run-up heights in meters. The parameters of this feature were used by Matt Hornbach at UTIG in tsunami modeling of the 1918 event.



the 4-6 m-high tsunami that inundated the northwest coast of Puerto Rico.

Colleagues at UTIG used the parameters of this feature in numerical tsunami modeling software, and determined a feature this size and this close to shore (approximately 18 km from Aguadilla) is capable of generating a 4-6 m-high tsunami that matches well with the observed run-up, phase, and timing (Hornbach et al., 2007).

Tappin et al. (2000) noted that, while much less common than fault-related seafloor displacement-induced tsunamis, fine-grained material that moves cohesively down slope, which is most typical of rotational slumps, can generate tsunamis. However, the main problem with modeling tsunamis generated by submarine slope failures are the rapid attenuation of the wave as it diverges spherically from the source. This phenomenon frequently causes the waves to match well with observations in near-field areas, but poorly in far-field areas (Hornbach et al., 2007).

The numerical modeling match of the feature in the southern Mona Canyon, and well as the occurrence of similar features throughout the study area indicates that submarine mass wasting along the steep slopes of the Mona Canyon poses a tsunami hazard to Puerto Rico. The parameters of mass wasting features visible throughout the Mona Canyon, such as the coordinates, size, shape, and approximate mass transport directions, may be used for re-evaluating and remodeling the 1918 tsunami. Ultimately, additional multi-channel seismic data focused specifically over the southern Mona Canyon to precisely locate the deposit from this slope failure, detailed volume calculations, coring and dating of the deposit, and more detailed tsunami modeling will be necessary to determine if the mass wasting feature in the southern Mona Canyon is a likely source mechanism for the 1918 tsunami.

CONCLUSIONS

- 1) Marine geophysical data presented in this study suggests that the Mona Canyon is a tectonically controlled submarine canyon, and has a significantly different morphology and structure than other typical submarine canyons. It can be separated into three structural domains: the southern, central, and northern Mona Canyon domains, the latter of which includes the Mona Block. The seismic reflection data suggests that the listric Mona Canyon master fault on the north and east side of the canyon, and antithetic faults on the south and west side of the canyon in the southern and central domains produce a half-graben structure. The northern Mona Canyon is also likely fault-controlled, however, its morphology suggests mass wasting has accentuated the bathymetric expression of this domain. The Mona Block is a region of post-Pliocene forearc uplift from the oblique subduction of the Bahamas platform. Potential evidence for this uplift includes NE-SW directed folding of the sedimentary cover in the central Mona Canyon, thrust faults in the metamorphic basement rock, and an observable cluster of shallow crustal earthquakes. Active faults in the study area are dominantly north- and northwest-trending normal and sinistral strike-slip faults, having maximum vertical components of dip separation of 3.5 km on the Mona Canyon Fault.
- 2) The Mona Canyon is older than the 1.2 million year age previously determined using GPS velocities in the northern Mona Passage. The marine geophysical data and balanced structural cross-section restoration presented in this study suggest that extension in the Mona Canyon began in the Middle Oligocene approximately 30 Ma and continues through the Recent. The minimum extension in the Mona

Canyon is interpreted to be 6.05 km, 4.39 km of which may have occurred from the Late Miocene through the Recent. The proposed cause of the 0.087 mm/year initial rifting, Phase I, may have been from seafloor spreading in the Cayman trough and/or sinistral strike-slip along the GSPRFZ beginning approximately 30 Ma. The collision of the Bahamas platform with the northern margin of Puerto Rico, which may have subsequently caused the $24^{\circ} \pm 5.8^{\circ}$ counterclockwise rotation of Puerto Rico, is proposed to have initiated the later, more rapid, 0.4 mm/year stage of extension, Phase II.

- 3) The pinning and extension model is the currently compatible tectonic model for the formation of the Mona Canyon. The rotating block and the incised canyon models may have had partial impacts on the deformation in the study area, via counterclockwise rotation and headward erosion, respectively, but are insufficient to account for all the evidence presented in the marine geophysical data.
- 4) This study presents evidence for a large, greater than 5 km^3 submarine mass wasting feature in the southern Mona Canyon that is located in the same region as two submarine cable breaks that occurred during the 1918 earthquake and tsunami. The location and parameters the mass wasting feature in the southern Mona Canyon can be used in tsunami modeling for the 1918 event, and hazard analyses for the northwest coast of Puerto Rico. However, additional multi-channel seismic data focused specifically over this area to precisely locate the deposit, detailed volume calculations, coring and dating of the deposit, and more detailed tsunami modeling will be necessary to determine if it is a likely source mechanism for the 1918 tsunami.

REFERENCES

- Boynton, C.H., Westbrook, G.K., Rott, M.H.P., Long, R.E., 1979. A seismic refraction investigation of the crustal structure beneath the Lesser Antilles island arc. *Geophys. J. R. Astron. Soc.*, 58, 371-393.
- Briggs, R.P., 1961. Geology of Kewanee Interamerican Oil Company test well number CPR-4, northern Puerto Rico, in: *Oil and Gas Possibilities of northern Puerto Rico*. Puerto Rico Mining Commission, San Juan, pp.1-23.
- Calais, E., Mazabraud, Y., Mercier de Lepinay, B., Mann, P., Mattioli, G., Jansma, P., 2002. Strain partitioning and fault slip rates in the northeastern Caribbean from GPS measurements. *Geophys. Res. Lett.*, 29, 3-1-3-4.
- Dolan, J., Mann, P., de Zoeten, R., Heubeck, C., Shiroma, J., Monechi, S., 1991. Sedimentologic, stratigraphic, and tectonic synthesis of Eocene-Miocene sedimentary basins, Hispaniola and Puerto Rico, in: Mann, P., Grenville, D., Lewis J.F. (Eds.), *Geologic and Tectonic Development of the North America-Caribbean Plate Boundary in Hispaniola*, *Geol. Soc. Am. Sp. Pap.* 262. *Geol. Soc. Am.*, Boulder, CO, pp.217-263.
- Dolan, J.F., Mullins, H.T., Wald, D.J., 1998. Active tectonics of the north-central Caribbean: Oblique collision, strain partitioning, and opposing subducted slabs, in: Dolan, J.F., Mann, P. (Eds.), *Active Strike-Slip and Collisional Tectonics of the Northern Caribbean Plate Boundary Zone*, *Geol. Soc. Am. Sp. Pap.* 326. *Geol. Soc. Am.*, Boulder, CO, pp.1-61.
- Dobson, M.R., Karl, H.A., Vallier, T.L., 1996. Sedimentation along the fore-arc region of the Aleutian Island Arc, Alaska, in: Gardner, J.V., Field, M.E., Twichell, D.C. (Eds.), *Geology of the United States' Seafloor: The View from GLORIA*. Cambridge Univ. Press, New York, NY, pp.279-304.
- Doser, D.I., Rodriguez, C.M., Flores, C., 2005. Historical earthquakes of the Puerto Rico-Virgin Islands region (1915-1963), in: Mann, P. (Ed.), *Active Tectonics and Seismic Hazards of Puerto Rico, the Virgin Islands, and Offshore Areas*, *Geol. Soc. Am. Sp. Pap.* 385. *Geol. Soc. Am.*, Boulder, CO, pp.103-114.
- Edgar, N.T., Parson, L.M., Dillon, W.P., Jacobs, C., Scanlon, K.M., Holcombe, T.L., 1989. Central Cayman trough: Gloria mosaic, interpretation, and track map. U.S. *Geol. Surv. Misc. Field Studies*, Map MF-2083, scale 1:375,000.
- Erikson, J.P. and Pindell, J.L., 1991. Fault zone deformational constraints on Paleogene tectonic evolution in southern Puerto Rico. *Geophys. Res. Lett.*, 18, 569-572.

- Fossen, H., Hesthammer, J., Johansen, T.E.S., Sygnabere, T.O., 2003. Structural geology of the Huldra Field, northern North Sea – a major tilted fault block at the eastern edge of the Horda Platform. *Mar. Pet. Geol.*, 20, 1105-1118.
- Fox, P.J., and Heezen, B.C., 1975. Geology of the Caribbean Crust, in: Nairn, A., and Stehil, F., (Eds.), *The Ocean Basins and Margins*, v.3. Plenum Press, New York, NY, pp.421-466.
- Gardner, W.D., Glover, L.K., Hollister, C.D., 1980. Canyons off northwest Puerto Rico: studies of their origin and maintenance with the nuclear research submarine NR-1. *Mar. Geol.*, 37, 41-70.
- Geist, E.L., Childs, J.R., Scholl, D.W., 1988. The origin of summit basins of the Aleutian Ridge: implications for block rotation of an arc massif. *Tectonics*, 7, 327-341.
- Gibbs, A.D., 1983. Balanced cross-section restoration from seismic sections in areas of extensional tectonics. *J. Struct. Geol.*, 5, 153-160.
- Gonzalez, L.A. and Ruiz, H.M., 1991. Diagenesis of middle Tertiary carbonates in the Toa Baja well, Puerto Rico. *Geophys. Res. Lett.*, 18, 513-516.
- Grindlay, N.R., Mann, P., Dolan, J.F., van Gestel, J.P., 2005. Neotectonics and subsidence of the northern Puerto Rico-Virgin Islands margin in response to the oblique subduction of high-standing ridges, in: Mann, P. (Ed.), *Active Tectonics and Seismic Hazards of Puerto Rico, the Virgin Islands, and Offshore Areas*, *Geol. Soc. Am. Sp. Pap.* 385. *Geol. Soc. Am.*, Boulder, CO, pp.31-60.
- Groshong, R.H., 1989. Half-graben structures: Balanced models of extensional fault-bend folds. *Geol. Soc. Am. Bull.*, 101, 96-105.
- Haq, B.U., Hardenbol, J., Vail, P.R., 1987. Chronology of fluctuating sea levels since the Triassic. *Science*, 235, 1156-1167.
- Heezen, B.B., Nesteroff, V., Rawson, M., Freeman-Lynde, R.P., 1985. Visual evidence for subduction in the western Puerto Rico trench. *Geodynamiques des Caribes*, Symposium Paris, 5-8 Fevrier: Editions Technip, 27, Rue GINOUX, 75015, Paris, France.
- Heezen, B.C. and Ewing, M., 1952. Turbidity currents and submarine slumps and the 1929 Grand Banks earthquake. *Am. J. Sci.*, 250, 849-873.
- Heinrich, P., Piatanesi, A., Herbert, H., 2001. Numerical modeling of tsunami generation and propagation from submarine slumps: the 1998 Papua New Guinea event. *Geophys. J. Int.*, 145, 97-111.

- Hippolyte, J.-C., Mann, P., Grindlay, N.R., 2005. Geologic evidence for the prolongation of active normal faults of the Mona Canyon into northwestern Puerto Rico, in: Mann, P. (Ed.), *Active Tectonics and Seismic Hazards of Puerto Rico, the Virgin Islands, and Offshore Areas*, Geol. Soc. Am. Sp. Pap. 385. Geol. Soc. Am., Boulder, CO, pp.161-171.
- Hornbach, M.J., Fronlich, C., Mann, P., Mondziel, S., Grindlay, N., 2007. Tsunami potential offshore northwest Puerto Rico II: Reevaluating the source of the 1918 Puerto Rico Tsunami. Geol. Soc. Am. Fall 2007 Annual Meeting, Abstracts with Programs, 38, 159.
- Hossack, J.R., 1979. The use of balanced cross-sections in the calculation of orogenic contraction: A review. *J. Geol. Soc. London*, 136, 705-711.
- Itturalde-Vinent, M.A. MacPhee, R.D.E., 1999. Paleogeography of the Caribbean region: Implications for Cenozoic Biogeography. *Bull. Am. Mus. Nat. Hist.*, 238, 95 pages.
- Jansma, P., Mattioli, G., Lopez, A., DeMets, C., Dixon, T., Mann, P., Calais, E., 2000. Neotectonics of Puerto Rico and the Virgin Islands, northeastern Caribbean from GPS geodesy. *Tectonics*, 19, 1021-1037.
- Joyce, J.J., 1991. Blueschist metamorphism and deformation of the Samana Peninsula: A record of subduction and collision in the Greater Antilles, in: Mann, P., Grenville, D., Lewis J.F. (Eds.), *Geologic and Tectonic Development of the North America-Caribbean Plate Boundary in Hispaniola*, Geol. Soc. Am. Sp. Pap. 262. Geol. Soc. Am., Boulder, CO, pp.47-76.
- Ladd, J.W., Worzel, J.L., Watkins, J.S., 1977. Multifold seismic reflection records from the northern Venezuela basin and the north slope of Muertos trench, in: Talwani, M., Pitman, W.C. III (Eds.), *Island Arcs, Deep-Sea Trenches, and Back-Arc Basins*. AGU, Washington, D.C., p.41-56.
- Ladd, J.W., Holcombe, T.L., Westbrook, G.K., Edgar, N.T., 1990. Caribbean marine geology; Active margins of the plate boundary, in: Dengo, G., Case, J.E. (Eds.), *The Geology of North America, v.H., The Caribbean Region*. Geol. Soc. Am., Boulder, CO, pp.261-290.
- LaForge, R.C., and McCann, W.R., 2005. A seismic source model for Puerto Rico, for use in probabilistic ground motion hazard analyses, in: Mann, P. (Ed.), *Active Tectonics and Seismic Hazards of Puerto Rico, the Virgin Islands, and Offshore Areas*, Geol. Soc. Am. Sp. Pap. 385. Geol. Soc. Am., Boulder, CO, pp.223-248.
- Larue, D.K., and Ryan, H.D., 1989. Extensional tectonism in the Mona Passage, Puerto Rico and Hispaniola: a preliminary study. *Transactions of the 12th Caribbean Geological Conference*, St. Croix, United States Virgin Islands. 223-230.

- Larue, D.K., 1991. The Toa Baja drilling project, Puerto Rico: Scientific drilling into a non-volcanic island arc massif. *Geophys. Res. Lett.*, 18, 489-492.
- Larue, D.K., and Ryan, H.F., 1998. Seismic reflection profiles of the Puerto Rico trench: Shortening between the North American and Caribbean plates, in: Lidiak, E.G., Larue, D.K. (Eds.), *Tectonics and Geochemistry of the Northeastern Caribbean*, Geol. Soc. Am. Sp. Pap. 322. Geol. Soc. Am., Boulder, CO, pp.193-210.
- Larue, D.K., Torrini, R., Smith, A.L., Joyce, J., 1998. North Coast Tertiary basin of Puerto Rico: From arc basin to carbonate platform to arc-massif slope, in: Lidiak, E.G., Larue, D.K. (Eds.), *Tectonics and Geochemistry of the Northeastern Caribbean*, Geol. Soc. Am. Sp. Pap. 322. Geol. Soc. Am., Boulder, CO, pp.155-176.
- Laursen, J., and Normark, W.R., 2002. Late Quaternary evolution of the San Antonio Submarine Canyon in the central Chile forearc (approximately 33°S). *Mar. Geol.*, 188, 365-390.
- Lewis, J.F. and Draper, G., 1990. Geology and tectonic evolution of the northern Caribbean margin, in: Dengo, G., Case, J.E. (Eds.), *The Geology of North America*, v.H., The Caribbean Region. Geol. Soc. Am., Boulder, CO, p.77-140.
- Macdonald, K.C. and Holcombe, T.L., 1978. Inversion of magnetic anomalies and seafloor spreading in the Cayman trough. *Earth Planet. Sci. Lett.*, 40, 407-414.
- MacPhee, R.D.E., Iturrelade-Vinent, Gaffney, E.S., 2003. Domo de Zaza, and Early Miocene vertebrate locality in south-central Cuba, with notes on the tectonic evolution of Puerto Rico and the Mona Passage. *Am. Mus. Novit.*, 3394, 42 pages.
- Mann, P., Calais, E., Ruegg, J.C., DeMets, C., Jansma P.E., Mattioli, G.S., 2002. Oblique collision in the northeastern Caribbean from GPS measurements and geological observations. *Tectonics*, 6, 1-23.
- Mann, P., 2005. Introduction, in: Mann, P. (Ed.), *Active Tectonics and Seismic Hazards of Puerto Rico, the Virgin Islands, and Offshore Areas*, Geol. Soc. Am. Sp. Pap. 385. Geol. Soc. Am., Boulder, CO, pp.1-12.
- Mann, P., Prentice, C.S., Hippolyte, J.-C., Grindlay, N.R., Abrams, L.J., Lao-Davila, D., 2005. Reconnaissance study of Late Quaternary faulting along Cerro Goden fault zone, western Puerto Rico, in: Mann, P. (Ed.), *Active Tectonics and Seismic Hazards of Puerto Rico, the Virgin Islands, and Offshore Areas*, Geol. Soc. Am. Sp. Pap. 385. Geol. Soc. Am., Boulder, CO, pp.115-137.

- Masson, D.G., and Scanlon, K.M., 1991. The neotectonic setting of Puerto Rico. *Geol. Soc. Am. Bull.*, 103, 144-154.
- McCann, W.R., and Sykes, L.R., 1984. Subduction of aseismic ridges beneath the Caribbean plate; implications for the tectonics and seismic potential of the northeast Caribbean. *J. Geophys. Res.*, 6, 4493-4519.
- McCann, W.R., 2002. Microearthquake data elucidate details of Caribbean subduction zone. *Seismol. Res. Lett.*, 73, 25-32.
- Mercado, A., and McCann, W.R., 1998. Numerical simulation of the 1918 Puerto Rico tsunami. *Nat. Haz.*, 18, 57-76.
- Mondziel, S.A., Grindlay, N.R., Mann, P., Hornbach, M.J., 2007. Tsunami potential offshore northwest Puerto Rico I: Mapping active faults and mass wasting features in the Mona Canyon. *Geol. Soc. Am. Fall 2007 Annual Meeting Programs with Abstracts*, 39, 159.
- Monroe, W.H., 1980. Geology of the Middle Tertiary formations of Puerto Rico. *U.S. Geol. Surv. Prof. Pap.*, 953, 93 pages.
- Moore, D.G., Curray, J.R., Einsele, G., 1982. Salado-Vinorama submarine landslide and turbidity current off the southeast tip of Baja California, in: Curray, J.R., Blakeslee, J., Platt, L.W., Stout, L.N., Moore, D.G., Aguayo, J.E., Aubry, M.-P., Gerhard, E., Fornari, D.J., Gieskes, J.M., Guerrero-Garcia, J., Kastner, M., Kelts, K.R., Lyle, M., Matoba, Y., Molina-Cruz, A., Niemitz, J., Rueda-Gaxiola, J., Saunders, A.D., Schrader, H., Simoneit, B.R.T., Vacquier, V. (Eds.), *Initial reports of the Deep Sea Drilling Project covering Leg 64 of the cruises of the drilling vessel Glomar Challenger, Mazatlan, Mexico to Long Beach, California, December 1978-January 1979, v.LXIV, part 2, pp.1071-1081.*
- Officer, C.B., Ewing, J.I., Hennion, J.F., Harkrider, D.G., Miller, D.E., 1959. Geophysical investigations in the eastern Caribbean: summary of the 1955 and 1956 cruises. *Phys. Chem. Earth*, 3, 17-109.
- Perfit, M.R., Heezen, B.C., Rawson, M., Donnelly, T.W., 1980. Chemistry, origin, and tectonic significance of metamorphic rocks from the Puerto Rico trench. *Mar. Geol.*, 34, 125-156.
- Pindell, J.L. and Barrett, S.F., 1990. Geological evolution of the Caribbean region; A plate tectonic perspective, in: Dengo, G., Case, J.E. (Eds.), *The Geology of North America, v.H., The Caribbean Region. Geol. Soc. Am., Boulder, CO, pp.405-432.*
- Reid, J.A., Plumley, P.W., Schellekens, J.H., 1991. Paleomagnetic evidence for Late Miocene counterclockwise rotation of north coast carbonate sequence, Puerto Rico. *Geophys. Res. Lett.*, 18, 565-568.

- Reid, H., and Taber, S., 1919. The Puerto Rico earthquakes of October-November 1918. *Seismol. Soc. Am. Bull.*, 9, 95-127.
- Rosencratz, E., Ross, M.I., Sclater, J.G., 1988. Age and spreading history of the Cayman trough as determined from depth, heat flow, and magnetic anomalies. *J. Geophys. Res.*, 93, 2141-2157.
- Sclater, J.G. and Christie, P.A.F., 1980. Continental stretching: an explanation of the post mid-Cretaceous subsidence of the central North Sea basin. *J. Geophys. Res.*, 85, 3711-3739.
- Shepard, F.P., 1981. Submarine canyons: Multiple causes and long-time persistence. *Am. Assoc. Pet. Geol. Bull.*, 65, 1062-1077.
- Talwani, M., Sutton, G.H., Worzel, J.L., 1959. A crustal cross-section across the Puerto Rico trench. *J. Geophys. Res.*, 65, 1545-1555.
- Tappin, D.R., Matsumoto, T., Watts, P., Satake, K., McMurtry, G.M., Matsumayama, M., Lafoy, Y., Tsuji, Y., Kanamatsu, T., Lus, W., Iwabuchi, Y., Yeh, H., Matsumoto, Y., Nakamura, M., Mahoi, M., Hill, P., Crook, K., Anton, L., Walsh, J.P., 1999. Sediment slump likely caused 1998 Papua New Guinea Tsunami. *Eos*, 80, 329, 334, 340.
- Tappin, D.R., Watts, P., McMurtry, G.M., Lafoy, Y., Matsumoto, T., 2000. The Sissano, Papua New Guinea tsunami of July 1998 – offshore evidence and the source mechanism. *Mar. Geol.*, 175, 1-23.
- van Gestel, J.-P., Mann, P., Dolan, J.F., Grindlay, N.R., 1998. Structure and tectonics of the upper Cenozoic Puerto Rico-Virgin Islands carbonate platform as determined from seismic reflection studies. *J. Geophys. Res.*, 103, 30505-30530.
- van Gestel, J.-P., Mann, P., Grindlay, N.R., Dolan, J.F., 1999. Three-phase tectonic evolution of the northern margin of Puerto Rico as inferred from an integration of seismic reflection, well, and outcrop data. *Mar. Geol.*, 161, 257-286.
- Wadge, G. and Burke, K., 1983. Neogene Caribbean plate rotation and associated Central American tectonic evolution. *Tectonics*, 2, 633-643.
- Western Geophysical, 1974. Offshore geophysical investigations for siting of a nuclear power station on Puerto Rico, for Puerto Rico Water Resources Authority. Preliminary Safety Analysis Report, US Atomic Energy Commission, Docket No. 50-376, North Coast Nuclear Plant No. 1, v.III, 101 pages.

Wu, S., Yu, Z., Zhang, R., Han, W., Zou D., 2005. Mesozoic-Cenozoic tectonic evolution of the Zhuanghai area, Bohai-Bay basin, east China: the application of balanced cross-sections. *J. Geophys. Eng.*, 2, 158-168.

Xiao, H. and Suppe, J., 1992. Origin of Rollover. *Am. Assoc. Pet. Geol. Bull.*, 76, 509-529.